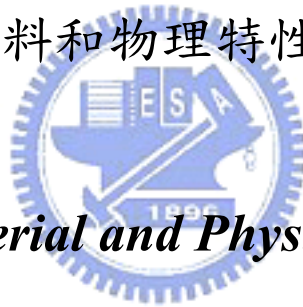


國立交通大學

電子物理研究所

碩士論文

利用溶膠旋轉塗佈法備製鈦酸鈷高介電層
與其材料和物理特性之研究



*A Study on Material and Physical Properties of
CoTiO₃ High-κ Dielectric Prepared by
Sol-Gel Spin Coating Method*

研究生：高國興

指導教授：趙天生 博士

中華民國九十七年

利用溶膠旋轉塗佈法備製鈦酸鈷高介電層

與其材料和物理特性之研究

A Study on Material and Physical Properties of

CoTiO₃ High-κ Dielectric Prepared by

Sol-Gel Spin Coating Method

研究生：高國興

Student : Kuo-Hsing Kao

指導教授：趙天生 博士

Advisor : Dr. Tien-Sheng Chao



Submitted to Institute of Electrophysics

College of Science

National Chiao Tung University

in Partial Fulfillment of the Requirements

for the Degree of Master of Science in Electrophysics

February 2008

Hsinchu, Taiwan, Republic of China.

中華民國 九十七 年

***A Study on Material and Physical Properties of
CoTiO₃ High- κ Dielectric Prepared by
Sol-Gel Spin Coating Method***

Student : Kuo-Hsing Kao

Advisors : Dr. Tien-Sheng Chao

**Institute of Electrophysics
National Chiao Tung University**

Abstract

In this thesis we form the high- κ dielectric CoTiO₃ by sol-gel spin coating method followed by different annealing temperature 600~900°C. The image of transmission electron microscopy (TEM) reveals that 2.2 nm interfacial layer is between Si-sub and CoTiO₃ annealed at 400°C. According to X-ray diffraction (XRD) analysis, crystallization temperature of the spin-on dielectric is between 600 and 700°C. Scanning probe microscope (SPM) describes surface morphology of the spin-on dielectrics with different annealing temperature and the surface roughness abruptly increases as annealing temperature higher than 600 °C. Electron spectroscopy for chemical analysis (ESCA) shows that higher temperature annealing results in thicker interfacial layer and pure chemical bonding. Furthermore ESCA also confirms that the spin-on dielectric with 600°C annealing has atomic concentration ratio [Co]:[Ti]:[O]~1:1:3. The spin-on film CoTiO₃ with 600°C annealing has Schottky emission conduction mechanism for the TaN/ CoTiO₃/ Si-sub structure. And the trapping characteristics of spin-on film CoTiO₃ with 600°C annealing is affected by temperature, applied stress voltage and stress time.

High electrical permittivity ($k\sim 40.2$) of CoTiO₃ dielectric is extracted via the high resolution transmission electron microscopy (HR-TEM) image and $C-V$ curves.

In addition, the valence energy band offset between thermally grown SiO₂ and spin-on CoTiO₃ is about 4.0eV, which is detected by high resolution X-ray photoelectron spectroscopy (HR-XPS). The band energy gaps of thermally grown SiO₂ and spin-on CoTiO₃ are 9.0 and 2.2 eV, respectively. The energy band alignment of spin-on CoTiO₃ directly with SiO₂ and indirectly with Si is successfully determined in this thesis.



利用溶膠旋轉塗佈法備製鈦酸鈷高介電層

與其材料和物理特性之研究

研究生：高國興

指導教授：趙天生 博士

國立交通大學

電子物理研究所碩士班

摘要

在這篇論文裡，我們利用溶膠旋轉塗佈法備製具有高介電係數的鈦酸鈷 CoTiO_3 介電層，並且對 $600\sim 900^\circ\text{C}$ 不同溫度退火後的樣品做詳細的研究。穿透式電子顯微鏡(TEM)的影像顯示著， CoTiO_3 與矽基板之間經過四百度的氧化後會產生 2.2 奈米的間隙層(interfacial layer)。根據 X 光繞射(XRD)圖形分析可知，這塗佈上去的 CoTiO_3 介電層的結晶溫度大約介於六百到七百度之間。我們也利用掃描式探針顯微鏡(SPM)描繪出經過不同溫度退火的 CoTiO_3 介電層的表面形貌，而高於六百度退火的樣品，其表面粗糙度會有急遽上升的現象發生。化學分析電子能譜儀(ESCA)的結果顯示，較高溫度的退火會導致較厚的間隙層與較純的化學鍵結。而更進一步的 ESCA 分析確定了這塗佈上去並且經過六百度退火的介電層的原子濃度比例， $[\text{Co}]:[\text{Ti}]:[\text{O}]$ 約為 1:1:3。經過六百度退火的 CoTiO_3 的電子傳導性質，在氮化鈮(TaN)/ CoTiO_3 /矽基板這樣的結構中由蕭基發射機制主導。而經過六百度退火的 CoTiO_3 捕捉電子的特性會受到溫度、施加電壓與加電壓時間的影響。介電質 CoTiO_3 的高介電常數($k\sim 40.2$)是藉由高解析度 TEM 影像與電容電壓($C-V$)曲線求得。另外，我們利用高解析度 X 光電子能譜儀(HR-XPS)偵測出二氧化矽與 CoTiO_3 間的價帶能量差(ΔE_v)，其值大約為 4.0 電子伏特；二氧化矽與 CoTiO_3 的能隙(E_g)分別為 9.0 與 2.2 電子伏特。因此，在這篇論文中， CoTiO_3 與二氧化矽的直接校準， CoTiO_3 與 Si 的間接校準也就被成功地決定了！

誌謝

得之於人者太多，出之於己者太少！

趙天生老師是學生第一個要感謝的人。謝謝老師給學生這個機會在實驗室裡學習，並且指導與充實學生在專業知識上的本質學能，更令人感動的是，老師會主動關心學生的日常生活與家庭經濟狀況，並給予適當的協助。

再來要感謝博士班**陳建豪學長**與**馬鳴汶學長**。除了指導學弟課業上的問題外，兩位學長更在學弟心中建立起做研究的良好典範；做研究做事情要像建豪學長一樣全能，動手做實驗要像小馬學長一樣有拼勁！還要感謝**郭伯儀學長**帶領學弟縱情於山水之間，吃遍特殊的台灣道地小吃。也要感謝**羅文正學長**與**吳偉成學長**，大家一起打球、游泳、撞球，兩位學長都會裝軟弱，讓學弟有可怕的自信與成就感；兩位學長也非常照顧學弟，當學弟哭倒路邊他們都立即伸出援手給予安慰。雖然**呂宗宜學長**不常出現在實驗室，也要感謝學長時常給予實驗室經濟上的支援，讓實驗室的活動能夠成功地舉辦。

此外，還要感謝已順利畢業的碩士班**黃竣祥學長**，**黃彥學學長**，**謝佩珊學姊**，**彭武欽學長**、**周棟煥學長**、**陳煒昕學長**，謝謝學長姊們一年多來的指教。還要謝謝同學嘴砲**大宗諭**、**小邱德鑫**、**小白美君**、**阿壘宜憲**、**漢堡妍心**、**猴子明宏**以及**小飛俠久騰**，學弟花和尚**冠迪**、**小宗育**、**出男智盟**、**娘娘腔翊鴻**、**威娘威良**、**顏董榮家**，室友雄哥**張競之**、捲捲**蔡亞俊**、禾禾**張佳禾**、宿舍長**江欣哲**以及偷渡客**陳威凱**豐富了我碩士班三年的生活。

還要感謝**爺爺高全緒**、**媽媽王月華**以及**姑姑高清娟**的支持，讓我無後顧之憂地致力於碩士學位。還有拉拉**蔡姿婷**在身邊的陪伴，以後就一直牽牽手吧！

另外，要特別感謝中華民國中正國防幹部預備學校以及海軍軍官學校過去對學生的十年栽培！

此論文獻給以上諸位！

高國興

誌於 新竹交大

Contents

<i>Abstract</i>	V
<i>Abstract (Chinese)</i>	V
Acknowledgements (Chinese)	V
Contents	V
<i>Table Caption</i>	V
<i>Figure Caption</i>	V

Chapter 1 Introduction

<i>1.1 Motivation of High-κ Gate Dielectrics Project</i>	1
<i>1.2 Metal xide Material for High-κ Gate Dielectrics</i>	2
<i>1.3 Requirements for High-κ Gate Dielectrics</i>	3
<i>1.3.1 Permittivity and Barrier Height</i>	4
<i>1.3.2 Thermodynamic Stability on Silicon</i>	4
<i>1.3.3 Interface Quality</i>	5
<i>1.3.4 Film Morphology</i>	6
<i>1.3.5 Gate Compatibility</i>	7
<i>1.3.6 Process compatibility</i>	7
<i>1.4 Sol-Gel Spin Coating Method</i>	8
<i>1.5 ESCA Technique</i>	9

Chapter 2 Experimental Procedures

<i>2.1 Device Fabrication</i>	17
<i>2.2 Material and physical Properties Measurements</i>	18

Chapter 3 Material Properties

<i>3.1 Si-sub/CoTiO₃ Interface Quality</i>	20
<i>3.2 Surface Morphology</i>	20
<i>3.3 Composition Analysis</i>	21

3.3.1 Auger Electron Microscope analysis.....	21
3.3.2 Electron Spectroscopy for Chemical analysis.....	22

Chapter 4 Physical Properties

4.1 Dielectric Permittivity.....	35
4.2 C-V and I-V Characteristics.....	35
4.3 Current Transport Mechanism.....	36
4.4 Band Gap Energy and Band Alignment.....	36

Chapter 5 Conclusion

5.1 Conclusion.....	44
Reference.....	46
Publication List.....	48
Vita (Chinese).....	51



Table Caption

Chapter 1

Table 1.1 Basic conduction processes in insulator. (pp. 16)

Figure Caption

Chapter 1

Fig. 1.1 Moore's law for microelectronic industry. The exponential increase of transistors counts as a function of time for distinct generations of microelectronics has been realized. (pp. 11)

Fig. 1.2 Calculated (lines) and measured (dots) results for tunneling currents from inversion layers through oxides. (pp. 11)

Fig. 1.3 The frequency dependence of the real (ϵ_r') and imaginary (ϵ_r'') parts of the dielectric permittivity. In CMOS devices, ionic and electronic contributions are present. (pp. 12)

Fig. 1.4 The symmetric perovskite crystal structure (a) is not polarized when there is no applied electric field. And the applied field polarizes the structure (b). (pp. 12)

Fig. 1.5 XRD pattern of Ta thin film oxidized at 700 ° C for 1, 1.5, 2, 3 and 4 min. (pp. 13)

Fig. 1.6 The evolution of surface morphology resulted from thermal oxidation at 700 ° C for 1(a), 3(b) and 4(c) min. (pp. 14)

Fig. 1.7 Schematic of the relevant energy levels for XPS binding energy measurements. Note that a conduction specimen and spectrometer are in electrical contact and thus have common Fermi levels. (pp. 15)

Fig. 1.8 Illustration of band gap energy by O 1s or N 1s photoelectron energy loss spectrum. (pp. 15)

Chapter 2

Fig. 2.1 The key process flow of sol-gel spin coating CoTiO₃. (pp. 19)

Chapter 3

Fig. 3.1 TEM image of Al-electrode/1-coated CoTiO₃ thin film/bare Si structure. (pp. 24)

Fig. 3.2 Electron dispersive spectra (EDS), associated with the TEM image showed in Fig. 3.1, of the CoTiO₃ dielectric annealed at 400 ° C. (pp. 24)

Fig. 3.3 XRD Spectra of spin-on CoTiO₃ films. The marked peaks correspond to crystallized CoTiO₃ phases. (pp. 25)

Fig. 3.4 SPM images of spin-on CoTiO₃ films with various thermal treatments at (a) 200°C, (b) 400°C, (c) 600°C, (d) 700°C, (e) 800°C and (f) 900°C. The image size is 1 μm by 1 μm. (pp. 31)

Fig. 3.5 Surface roughness of spin-on dielectrics as functions of annealing temperature. (pp. 32)

Fig. 3.6 Auger depth profile of the CoTiO₃ dielectric annealed at 600°C. (pp. 32)

Fig. 3.7 ESCA spectra of Si 2*p*(a), O 1*s*(b), Co 2*p*(c) and Ti 2*p*(d) with different annealing temperature. (pp. 33)

Fig. 3.8 ESCA spectra of Co 2*p*(a), Ti 2*p*(b) and O 1*s*(c) for the spin-on dielectric annealed at 600°C. (pp. 34)

Chapter 4

Fig. 4.1 TEM micrograph of an ultrathin CoTiO₃ film spin-coated on a high quality thermal SiO₂ layer and annealed at 600°C. (pp. 38)

Fig. 4.2 *C-V* curves of capacitors with TaN/CoTiO₃/SiO₂/Si and TaN/SiO₂/Si stack structures. (pp. 38)

- Fig. 4.3 C - V curves of spin-on CoTiO_3 films with different thermal treatments. (pp. 39)
- Fig. 4.4 I - V curves of spin-on CoTiO_3 films with different thermal treatments. (pp. 39)
- Fig. 4.5 Effective oxide thickness and current density of spin-on dielectrics as functions of annealing temperature. (pp. 40)
- Fig. 4.6 I - V curves measured at RT and elevated temperatures. (Inset) Extracted Schottky-emission barrier heights. (pp. 41)
- Fig. 4.7 Effective barrier heights extracted from I - V curves by using Schottky-emission and Frenkel-Poole models. (pp. 41)
- Fig. 4.8 ESCA spectra of O $1s$ for thermally grown 15 nm- SiO_2 . (pp. 42)
- Fig. 4.9 ESCA spectra of O $1s$ for the spin-on 15 nm- CoTiO_3 dielectric annealed at 600°C . (pp. 42)
- Fig. 4.10 Maximum valence energy band spectra of thermally grown 15 nm- SiO_2 and spin-on 20 nm CoTiO_3 dielectric annealed at 600°C measured by high resolution ESCA. (pp. 43)
- Fig. 4.11 Band alignment between Si, SiO_2 and spin-on CoTiO_3 dielectric with 600°C annealing. (pp. 43)

Chapter 1

Introduction

In this chapter, the reasons for why traditional silicon dioxide should be replaced by high- κ gate dielectrics will be addressed. Then the fundamental properties of high- κ materials will be introduced. We will briefly illustrate the requirements for high- κ gate dielectrics. Finally, we will introduce the method of sol-gel spin coating used in this thesis and the ESCA analyzing technique.

1.1 Motivation of High- κ Gate Dielectrics Project

The speedy progress of complementary metal-oxide-semiconductor (CMOS) integrated circuit technology has made our chips more powerful, even cheaper and met several requirements. The requirements include higher speed, lower consumption, and so on. And these have been accomplished by scaling down the transistor feature size, such as channel length and gate silicon-oxide (SiO_2) thickness. According to Moore's law, an exponential growth in the number of transistors per chip was predicted and had been proven true as shown in figure 1.1 [1].

One reason that Si-based devices have played the main roles in microelectronic fabrication is that Si has a high quality and easily-formed SiO_2 . And it exhibits low trap density, large band gap, low interface state density, high carrier mobility and good thermal stability with Si. Unfortunately, significant gate leakage current increases and boron penetration occurs when SiO_2 is scaled less than 30\AA as shown in figure 1.2 [2]. However, a temporary solution, silicon nitride or oxynitride (SiO_xN_y), relaxes the problems. SiO_xN_y owns slightly higher dielectrics constant ($\kappa \sim 7.5$) and which reduces the gate leakage current due to thicker physical film. The particular Si-O-N network bonding in SiO_xN_y greatly suppresses boron penetration through the dielectrics. But, a further problem is that the dielectrics constant value of SiO_xN_y is

not high enough. And it is necessary to find a candidate material which has higher dielectric constant for replacing conditional gate dielectrics.

1.2 Metal Oxide Material for High- κ Gate Dielectrics

As the description in the classical electrostatics, the internal polarization \mathbf{P} of a substance is induced when an external electric field \mathbf{E} is applied on it. And which can be formulated simply as below equation,

$$\mathbf{D} = \epsilon_0 \mathbf{E} + \mathbf{P}, \quad (1-1)$$

where \mathbf{D} is the electric displacement and ϵ_0 is the permittivity of free space. However, we can rewrite Eq. (1-1) and replace the internal polarization \mathbf{P} by a coefficient κ called dielectric constant,



$$\mathbf{D} = \epsilon_0 \kappa \mathbf{E}. \quad (1-2)$$

Comparing Eq. (1-1) with Eq. (1-2), therefore, we know that dielectric constant κ is used to tell the degree of the polarization of certain material while the external electrical field is applied.

Figure 1.3 illustrates the relation between the real (ϵ_r') and imaginary (ϵ_r'') parts of the dielectric permittivity and the frequency, and also marks the current frequency range for CMOS operation (100MHz~10GHz) [3]. There are two main contributions to the dielectric constant which give rise to the polarization: electronic and ionic dipoles. In general, atoms with higher atomic number demonstrate more electron dipole response to an external electrical field, because there are more electrons to respond to the field. And this electronic contribution tends to increase the permittivity

at ultrahigh frequency ($\sim 10^{16}$ Hz) as a result of the light electrons.

The ionic contribution to the permittivity could be much larger than the electronic portion such as (Ba, Sr)TiO₃ which exhibits ferroelectric behavior (perovskite crystal structure) below Curie Temperature. As shown in figure 1.4, Ti ions in the unit cells are displaced in response to an applied electric field. This displacement of Ti ions results in a huge polarization in the material, and thus can give rise to large dielectric constants (SrTiO₃ ~ 175 [4]). Since ions respond more slowly than electrons to an applied field, the ionic contribution begins to decrease at very high frequency ($\sim 10^{12}$ Hz), as shown in Figure 1.3.

Furthermore, we can modify the polarization behavior of an insulator by low level incorporation. This low level incorporation actually changes the localized bonding order and the vibration mode of the network ions in that insulator. G. Lucovsky and B. Rayner demonstrated this phenomenon by low level doping Zr (or Hf) atoms in the SiO₂ film; and the dielectric constant of the insulator increased due to the discernable change in bonding order and in vibration modes [5].

In summary, we can briefly tell the main contributions to the polarization of insulators for gate dielectrics: electronic, ionic and low level incorporation. However, the above contributions will be distinguished when the atoms own more electrons and higher atomic number. And that's why metal oxide exhibits higher permittivity than the SiO₂.

1.3 Requirements for High- κ Gate Dielectrics

In order to successfully replace gate SiO₂, the alternative high- κ material should possess some required properties for next generation devices. In this section, we are going to talk about this issue.

1.3.1 Permittivity and Barrier Height

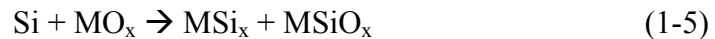
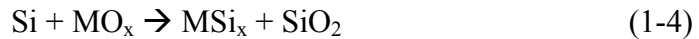
As previous discussion, an insulator with higher permittivity reduces the gate leakage current due to thicker physical thickness. However, leakage mechanism actually is dominated by intrinsic properties and is affected by extrinsic properties. The intrinsic properties of the insulator include band gap (E_g), the dielectric constant (κ) and the conduction band offset (ΔE_C). The extrinsic properties of the insulator include physical thickness, film morphology, the method of deposition, temperature and applied electrical field to the insulator. And several basic conduction processes in insulators are listed in table 1.1 [6].

Therefore, as described in table 1.1, the direct tunneling current will be obviously suppressed by increasing the physical thickness and the conduction band offset.

1.3.2 Thermodynamic Stability on Silicon

So far, most of the studied high- κ metal oxide systems have unstable interfaces with Si; they react with Si to form an undesirable interfacial layer. However, that will reduce the effective oxide thickness (E.O.T.) and degrade the carrier mobility under the interfacial layer [7]. So it is important to understand the thermodynamics of these systems and thereby attempt to control the interface with Si.

Because Si devices will undergo several high temperature processes after high- κ deposition on Si-sub, possible interfacial reaction are given as follows:



(M: metal, MO_x : high- κ metal oxide, MSi_x : metal silicide, MSiO_x : metal silicate)

Although the interfacial metal-silicon products are usually detrimental to the gate oxide performance, the metal silicate which is shown in Eq. (1-5) is even helpful in some aspects. Taking HfO_2 and HfSiO_4 for example, the interface and crystallization temperature of HfSiO_4 are sharper and higher than those of HfO_2 , respectively [7][8]. And we will discuss high- κ material crystallization temperature more detail later.

In addition to the issue of thermodynamics stability between high- κ material and bare Si-sub, the Eq. (1-6) describes that the excess oxygen atoms diffuse through the high- κ metal oxide and react with Si at high temperature. Especially in the ultra-thin film regime, this reaction will cause undesirable interfacial layer more easily.

Therefore, in order to precisely control the EOT of high- κ gate oxide and obtain better interface between gate oxide and Si-sub, we need to find certain high- κ metal oxide which has good thermodynamics stability with Si-sub at high temperature.

1.3.3 Interface Quality

A definite goal of any potential high- κ gate dielectric is to have a sufficiently high-quality interface with Si channel, as close as possible to that of SiO_2 . And the SiO_2 gate dielectric has a midgap interface state density $D_{it} \sim 2 \times 10^{10}$ states/cm² [6]. However, most of the investigated high- κ materials represent $D_{it} \sim 10^{11}$ - 10^{12} states/cm², and exhibit a flatband voltage shift $\Delta V_{FB} > 300\text{mV}$ [7]. Therefore, in order to obtain an optimal high- κ -Si interface quality, it is critical to understand the origin of the interface properties of any high- κ gate dielectric.

Because of the lattice structure mismatch, there certainly exists some interface defect states between high- κ gate oxide and Si-sub. It is empirically shown that if the average number of bonds per atom $N_{av} > 3$ at the interface, the interface defect density will increase proportionally, and the device performance will be degraded also. Metal oxides which contain elements with a high coordination, such as Ta and Ti, will have a high N_{av} , and form an overconstrained interface with Si. And degradation in leakage

current and electron channel mobility is also observed [9]. Furthermore, the silicide bonding which forms near the Si channel interface will tend to give rise to detrimental bonding conditions, leading to significant leakage current and poor carrier channel mobility.

As mentioned earlier in Eq. (1-6), oxygen atoms may diffuse through the high- κ dielectric and react with Si. And ZrO_2 and HfO_2 have been studied as having high oxygen diffusivities [10]. Although we know that there exists better interface between SiO_2 and Si-sub ($D_{it} \sim 2 \times 10^{10}$ states/cm²), an uncontrolled interfacial SiO_2 will severely compromise the capacitance gain from any high- κ material in that gate stack structure. Therefore, the character of resisting to oxygen diffusion in the annealing ambient should be considered when we are assessing the interface stability of high- κ dielectric.

Furthermore, the ideal gate dielectric stack may well turn out to have an interfacial layer composed of several monolayers of Si-O and a high- κ dielectric is used on the top of the interfacial layer. And this stack structure could possess better quality interface like that of SiO_2 and higher capacitance because of the high- κ material.

1.3.4 Film Morphology

The work by R. Chandrasekharan *et al.* investigated the film morphology of high- κ dielectric Ta_2O_5 and recognized the relation between oxidation time and crystallization temperature [11]. Figure 1.5 shows that no peak of crystalline Ta_2O_5 is observed until after 1.5min of oxidation. Between 1.5 and 2 min of oxidation, crystalline phases of Ta_2O_5 begin to appear. Furthermore, as the oxidation time increases, the intensity of crystal formation also increases. And figure 1.6 shows that the surface morphology of Ta_2O_5 film with different oxidation time. For the 1-min-oxidated sample, no change of surface morphology is observed; for the

3-min-oxidized sample, the surface becomes rough and small cracks start to appear while the oxide grains are formed; and the 4-min-oxidized one, the surface becomes rougher and more cracks are observed while larger grains are formed.

Because grain boundaries serve as highly leaky paths, it is expected to find a material which remains in an amorphous phase even if the film undergoes high temperature processes.

1.3.5 Gate Compatibility

As mentioned in 1.3.2, when high- κ materials directly contact with Si-sub, they will react with Si and form unfavorable interfacial layers. The similar reactions will also occur when high- κ materials meet poly-Si gate electrodes [12]. Furthermore, the dopant diffusion through high- κ gate dielectric will cause an unfavorable V_{th} shift [13][14]. And metal gate is one of possible solutions to suppressing dopant diffusion, poly depletion and sheet resistance constraint. In addition, the use of metal gates in gate processes can lower the thermal budget by eliminating the need for the dopant activation of poly-Si electrode [7].

Since doped poly-Si is the incumbent gate electrode material, it should be carried out to investigate how dopants in poly-Si diffuse through high- κ materials. However, current roadmap predicts that the metal gate technology will replace the doped poly-Si gates [15]. It is therefore necessary to focus efforts on dielectric materials systems which are compatible with potential metal gate materials.

1.3.6 Process Compatibility

There are several studying methods to deposit a high- κ dielectric: physical vapor deposition (PVD) [16], chemical vapor deposition (CVD) [12], molecular beam epitaxy (MBE) [4] and sol-gel spin coating method [17][18][19].

PVD principally includes evaporation and sputtering. Though these two PVD methods could be carried out at normal temperature for unlimited substrate materials,

the poor step coverage is the most challenge to deposit an uniform gate dielectric. In a sputtering process, however, the inevitable plasma damage results in surface damage and thereby creates unwanted interfacial states [7].

CVD mainly involves metal organic chemical vapor deposition (MOCVD) and atomic layer deposition (ALD). Though most of CVD methods have proven to give more uniform step coverage, the ALD method seems to provide much promise to deposit better-quality high- κ gate dielectrics than that of MOCVD. Furthermore, as far as the throughput and the requirements for instrument are concerned, it is obviously that ALD method is better than MOCVD and MBE methods [7].

This study mainly uses the sol-gel spin coating method to form the high- κ gate dielectrics. However, the more detail introduction about this method will be provided in the next section.



1.4 Sol-Gel Spin Coating Method

Recently, many technologies have been used to prepare various high- κ dielectrics, such as atomic layer deposition (ALD), chemical vapor deposition (CVD) and physical vapor deposition (PVD). Nevertheless, the sol-gel spin coating method also catches much attention; it is utilized to form the high- κ dielectric films [17] and memory charge trapping layers [18][19].

In the sol-gel processes, hydrolysis, condensation, and polymerization, the step-by-step formation leads to a metal-oxide network. And there is an arresting character of sol-gel spin coating method and which is an ability to synthesize new types of high- κ materials, called “inorganic-organic hybrid” [20].

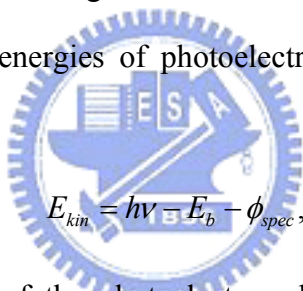
The sol-gel spin coating method could be executed in the normal pressure environment rather than high vacuum system. And thin film formation with spin coating is simpler than ALD, PVD, or MBE to deposit an insulator because of its

cheaper precursors and tools.

1.5 *Electron Spectroscopy for Chemical Analysis (ESCA)*

In this section it is worth introducing the fundamental principle of ESCA because the most following analysis for material and physical properties are performed by ESCA technique.

ESCA, also known as XPS, is used to characterize the chemical bonding and film composition. Since the photon energy range of interest for material analysis corresponds to the x-ray energy (1-10 keV), photoelectron spectra with specific binding energies produced by x-ray radiation of a sample present chemical bonding information about given elements. Figure 1.7 shows relevant energy levels for ESCA measurements [21]. Binding energies of photoelectrons can be obtained from Eq. (1-7), based on Figure 1.7.


$$E_{kin} = h\nu - E_b - \phi_{spec}, \quad (1-7)$$

where E_{kin} is kinetic energy of the photoelectron, h is Plank's constant, ν is the frequency of the photon, E_b is the binding energy, and ϕ_{spec} is the work-function of the spectrometer.

However the ejected photoelectrons from ESCA analysis undergo inelastic energy losses due to collective oscillations (plasmon) and single particle excitation (electron-hole band to band transitions). More importantly, the excitation of a single electron from the valence band to the conduction band can also be detected at the onset of plasma energy loss, as illustrated in Figure 1.8 [22]. This onset point of plasma energy loss can be utilized to determine the band gap energy [23-25]. Photo-excited electrons lose their kinetic energies due to collective oscillations of outer shells, resulting in a plasmon spectrum. Single electron excitation from valence

band edge to conduction band edge also takes place at the onset of a plasmon spectrum. E_c , E_v , E_g , and $h\nu$ denote conduction band minimum, valence band maximum, band gap energy, and photon energy of X-ray irradiation, respectively.



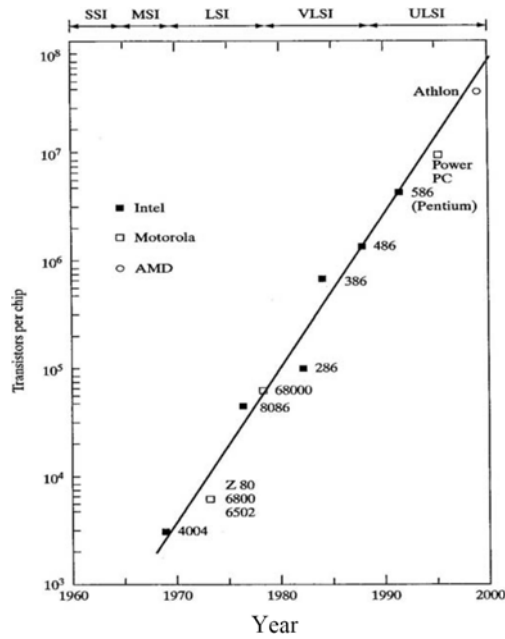


Figure 1.1 Moore's law for microelectronic industry. The exponential increase of transistors count as a function of time for distinct generations of microelectronics has been realized [1].

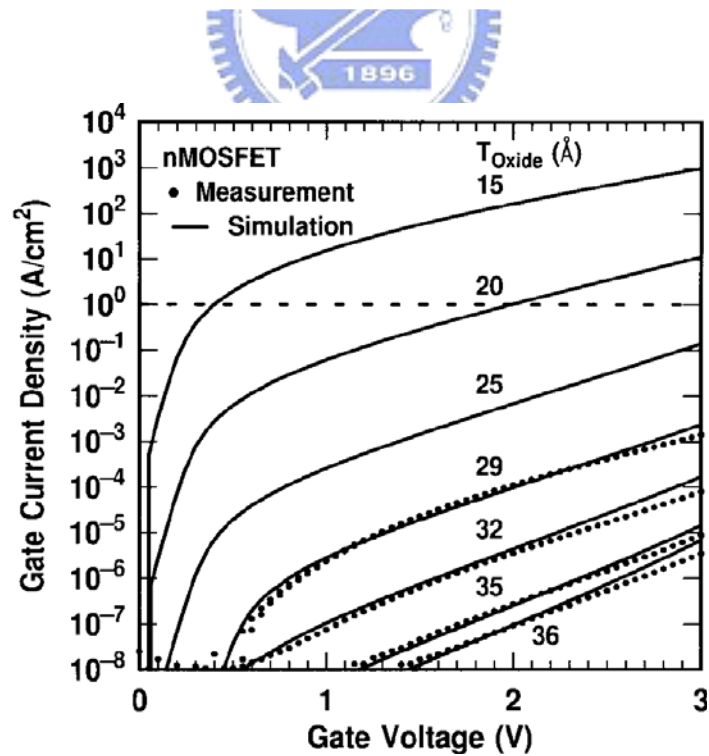


Figure 1.2 Calculated (lines) and measured (dots) results for tunneling currents from inversion layers through oxides [2].

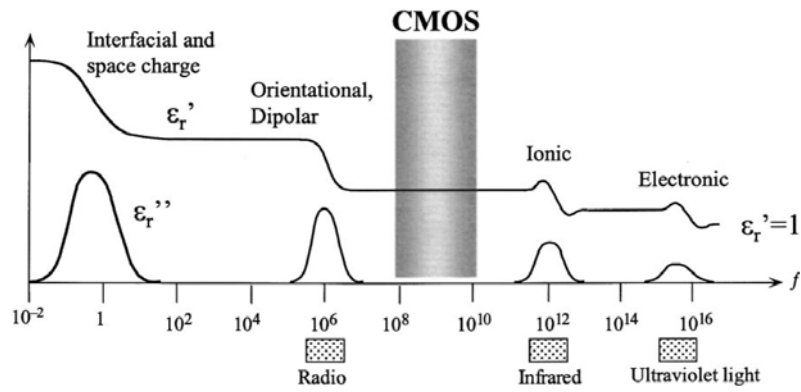


Figure 1.3 The frequency dependence of the real (ϵ_r') and imaginary (ϵ_r'') parts of the dielectric permittivity. In CMOS devices, ionic and electronic contributions are present.

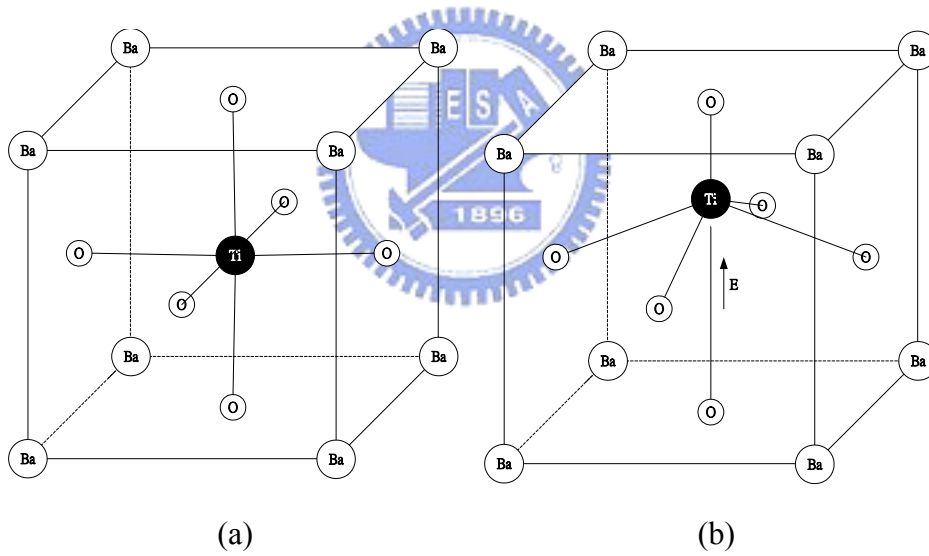


Fig. 1.4 The symmetric perovskite crystal structure (a) is not polarized when there is no applied electric field. And the applied field polarizes the structure (b).

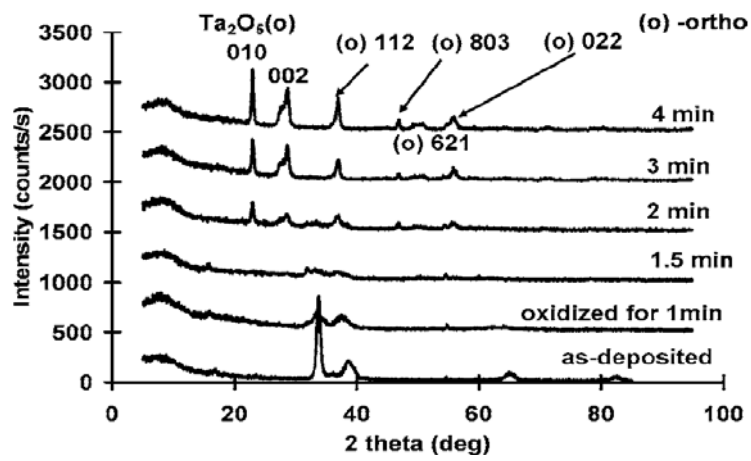


Fig. 1.5 XRD pattern of Ta thin film oxidized at 700 ° C for 1, 1.5, 2,3 and 4 min [11].



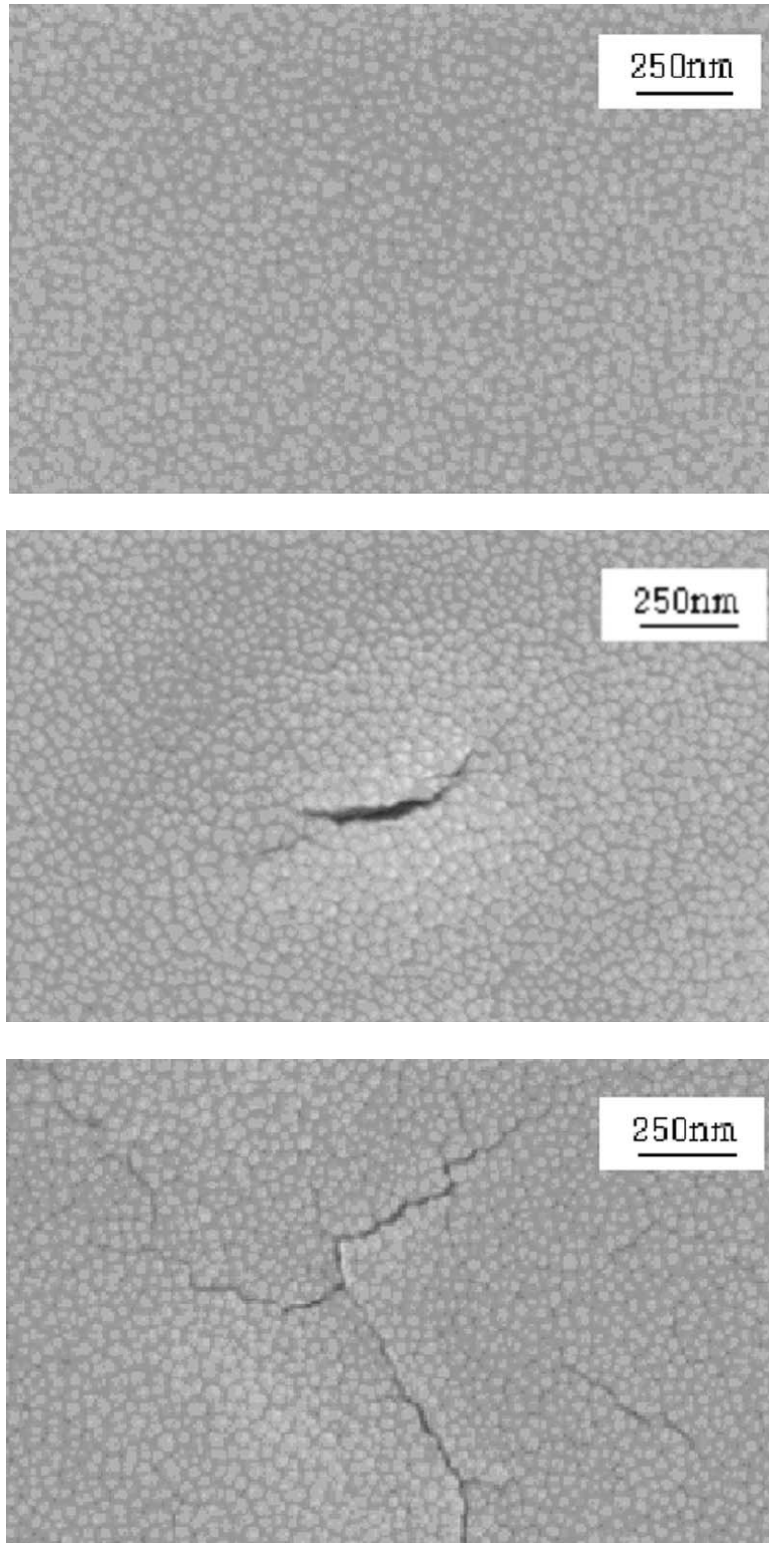


Fig. 1.6 The evolution of surface morphology resulted from thermal oxidation at 700 ° C for 1(a), 3(b) and 4(c) min [11].

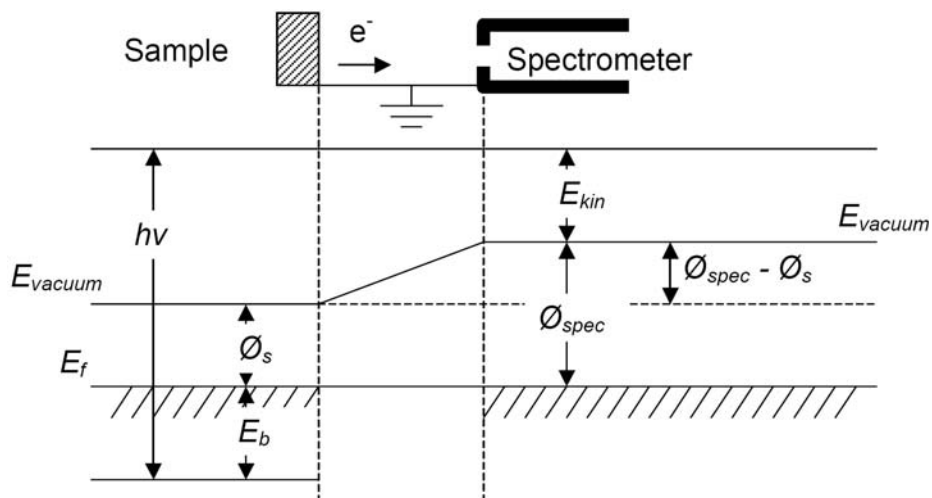


Fig. 1.7 Schematic of the relevant energy levels for XPS binding energy measurements. Note that a conducting specimen and spectrometer are in electrical contact and thus have common Fermi levels.

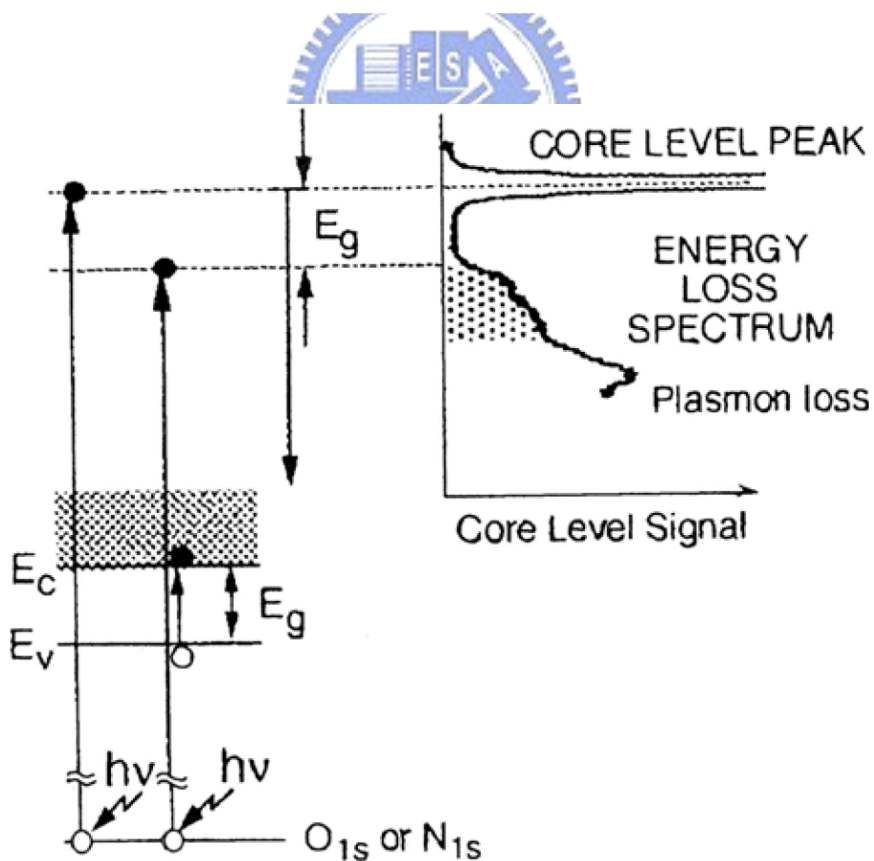


Fig. 1.8 Illustration of band gap energy by O 1s or N 1s photoelectron energy loss spectrum.

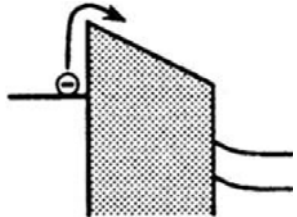
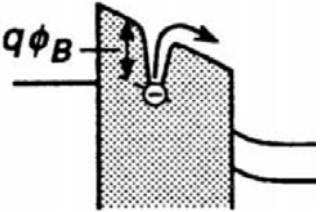
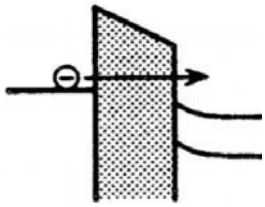
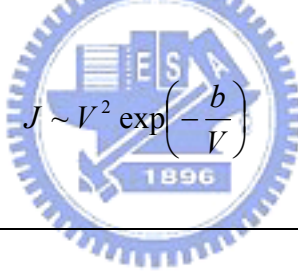
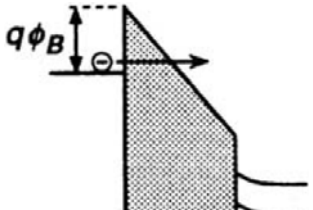
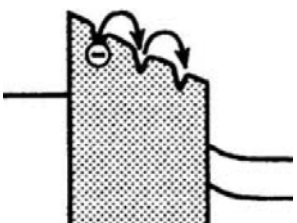
Schottky Emission	$J \sim T^2 \exp\left(\frac{+a\sqrt{V}}{T} - \frac{q\phi_B}{kT}\right)$	
Frenkel-Poole Emission	$J \sim V \exp\left(\frac{+2a\sqrt{V}}{T} - \frac{q\phi_B}{kT}\right)$	
Direct Tunneling	$J \sim \frac{1}{t_{diel}^2} \exp\left[-2t_{diel} \sqrt{\frac{2m^* q}{\hbar^2} \left(\Phi_B - \frac{V_{diel}}{2}\right)}\right]$	
Fowler-Nordheim Tunneling	 $J \sim V^2 \exp\left(-\frac{b}{V}\right)$	
Hopping (Ohmic) Conduction	$J \sim V \exp\left(-\frac{c'}{T}\right)$	

Table 1.1 Basic conduction processes in insulators [6].

Chapter 2

Experimental Procedures

In this chapter we will illustrate the device fabrication process with figures and list the instruments for material and physical properties measurements.

2.1 *Device Fabrication*

In this investigation, CoTiO₃ films were prepared by sol-gel spin coating method in a controlled environment, where was maintained at 22°C and 43 % RH. The process flow was illustrated in figure 1. First, n-type single crystal Si wafers with resistivity 4-7 Ωcm underwent standard RCA cleaning followed by a dilute-HF dip to remove the native SiO₂. Then, the sol-like precursor for CoTiO₃ was directly spun on the Si substrates at about 3000 revolutions per minute, and the spin speed was maintained for 30 seconds. However the precursor for cobalt and titanium elements were cobalt acetate tetrahydrate Co(OOCCH₃)₂ · 4H₂O and titanium isopropoxide Ti(OCHC₂H₆)₄, respectively. These two precursors were dissolved in 2-methoxyethanol for spin coating method. After the spin-coating of the precursor, in order to remove the solvent, the samples were baked at 90°C for 1.5 min on a hotplate. And the procedure (coating-and-baking) was repeated for 5 times. Afterward the films were oxidized at 400°C in an N₂/O₂ ambient for 10 min, in which both N₂ and O₂ flow were 50 sccm. In order to study the properties of CoTiO₃ high-*k* dielectrics after high temperature treatment, rapid thermal annealing (RTA) was performed. The samples were annealed at 600°C, 700°C, 800°C or 900°C for 30s in N₂ ambient. Photolithography was used to define gate areas and then TaN metal was deposited on the top of samples by reactive DC-sputtering. Lift-off was performed to form the MIS capacitors. Thereafter, ohmic contacts were formed by thermal evaporation of 300-nm-thick aluminum (Al) electrode on the backside of the samples.

2.2 *Material and Physical Properties Measurements*

The microstructure of spin-on CoTiO₃ film and Si substrate were studied by JEOL JEM-2100F field emission transmission electron microscopy (TEM) equipped with Link ISIS-300 energy dispersive X-ray analyzer (EDS). And the TEM EDS with a 5-nm electron beam probe was used to perform chemical analysis qualitatively.

The characteristic of crystallization of spin-on CoTiO₃ films with different annealing temperature were identified by PANalytical X'Pert Pro X-ray diffraction system under normal atmosphere. Optical module with X-ray mirrors and a parallel plate collimator was used to perform grazing incident X-ray diffraction (angle of incidence $\theta_i \sim 1^\circ$). The beam source originated from Cu $K\alpha$ radiation with a 0.154-nm wavelength and this beam source was operating at 1.8 kW.

Surface morphology of spin-on CoTiO₃ films with different annealing temperature was obtained by Veeco dimension 5000 scanning probe microscope (SPM) under normal atmosphere. The highest resolution in X-Y plane and Z direction were about 1.5 nm and few angstroms, respectively. And the tip curvature radius was about 2 nm.

A ULVAC-PHI Quantera high resolution X-ray photoelectron spectrometer (HR-XPS) with 180° spherical capacitor analyzer was used to analyze quantitatively the chemical composition of the dielectrics CoTiO₃ prepared by sol-gel coating method.

The capacitance-voltage ($C-V$) curves and current-voltage ($I-V$) curves were measured in the same probe station by HP 4284 and Keithly 4200, respectively.

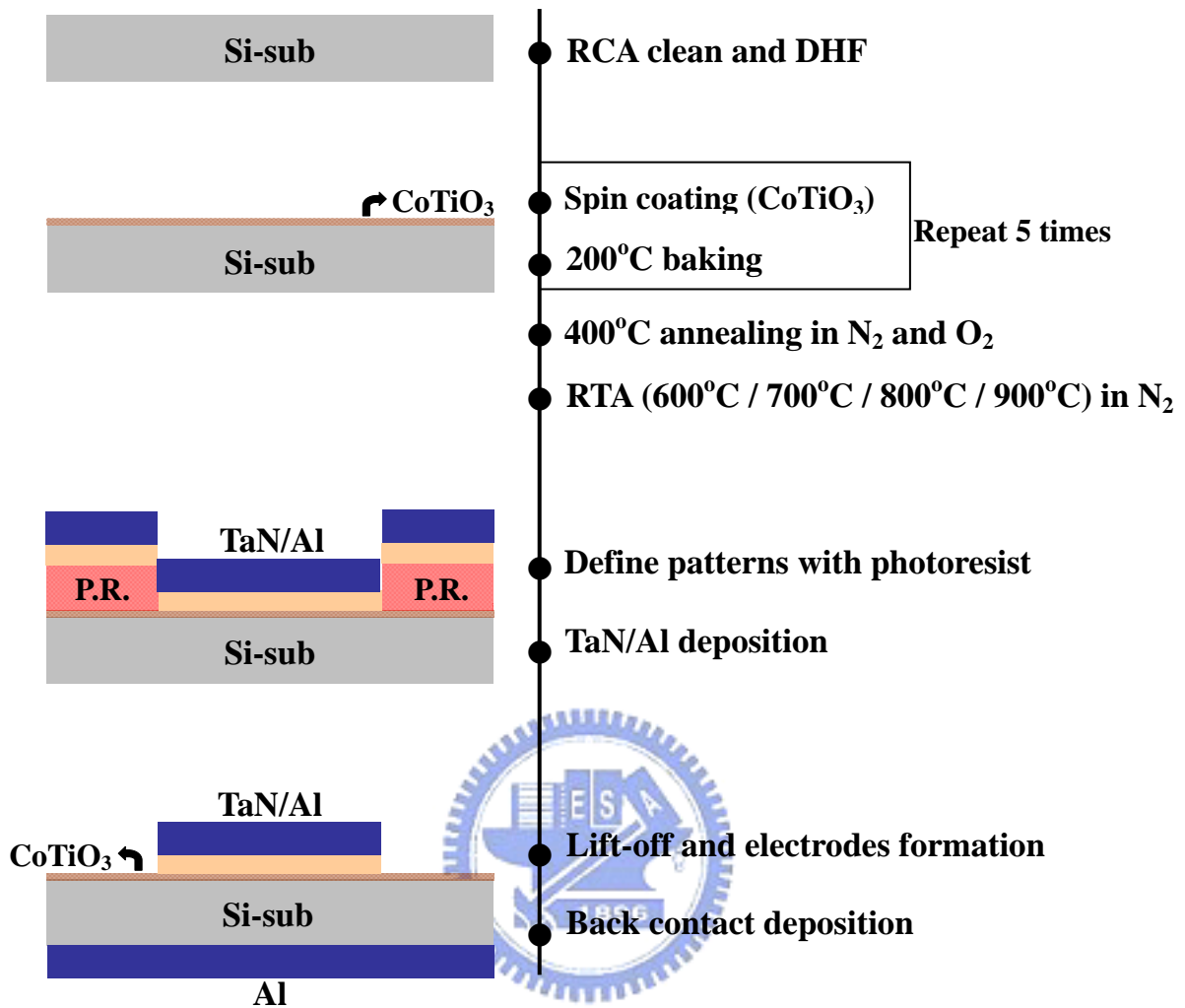


Fig. 2.1 The key process flow of sol-gel spin coating CoTiO_3 .

Chapter 3

Material Properties

In this chapter, we will report the material properties of spin-on CoTiO₃ thin films analyzed by Transmission Electron Microscope (TEM), Energy Dispersive Spectrometer (EDS), Grazing Incident X-Ray Diffraction (GI-XRD), Scanning Probe Microscope (AFM), Auger Electron Microprobe (AEM) and Electron Spectroscopy for Chemical Analysis (ESCA).

3.1 *Si-sub/CoTiO₃ Interface Quality*

In figure 3.1, the graph is the cross-section of Al-electrode/1-coated CoTiO₃ thin film/bare Si substrate structure and the CoTiO₃ thin film is annealed at 400°C. There are two interfacial layers astride the CoTiO₃ thin film. The interfacial layer between Si-sub and CoTiO₃ thin film is about 2.23 nm and the interfacial layer between Al-electrode and CoTiO₃ thin film is about 1.88 nm. Furthermore, the thickness of the 1-coated CoTiO₃ thin film on Si-sub is about 5.27 nm.

In order to qualitatively recognize the composition of the spin-on dielectric, EDS analysis is performed. As shown in figure 3.2 (a), the three principal elements, Cobalt, Titanium and oxygen, are detected. However, as shown in figure 3.2 (b), Al peak and Si peak maybe come from the interfaces beside the dielectric, and the Cu peak should be contributed to the Cu net which is used to hold the sample. Therefore there are three main elements, cobalt, titanium and oxygen in the spin-on dielectric.

3.2 *Surface Morphology*

As mentioned in section 1.3.4, it is desirable that the surface morphology of high-κ dielectric is still smooth though it undergoes high temperature treatment. PANalytical X'Pert Pro (XRD) and Veeco Dimension 5000 Scanning

Probe Microscope (D5000) are used to analysis surface morphology of films with different high temperature annealing.

Figure 3.3 presents the GI-XRD spectra of the CoTiO₃ thin films. No significant signals could be found for samples treated at temperatures below 600°C, indicating amorphous CoTiO₃ films to begin with. When a sample was annealed at a temperature above 700°C, signals of crystallized CoTiO₃ phases were found. This suggests the crystallization temperature of spin-on CoTiO₃ films being 600~700°C. Furthermore, signals of Si substrates were also found in the GI-XRD spectra for samples annealed at temperatures beyond 800°C. It is speculated that the crack of CoTiO₃ films has partially exposed the Si substrate after annealed at elevated temperatures.

Figure 3.4 shows the SPM images of CoTiO₃ films with different high temperature treatments. From figure 3.4(a) to figure 3.4(f) are the flattened and 3-D images of samples baked or annealed at 200°C, 400°C, 600°C, 700°C, 800°C, and 900°C, respectively. The extended dark regions was found in the images for 600~900°C annealed samples. Serious cracks of the CoTiO₃ thin film can be found after annealed at 900°C, as shown in figure 3.4(f). And figure 3.5 reports that the roughness of samples suddenly becomes serious when annealing temperature is higher than 600 °C.

3.3 Composition Analysis

3.3.1 Auger Electron Microscope Analysis

The incorporation of carbon element in a dielectric will decrease the effective dielectric constant [26]. Therefore Auger depth profile is used to analyze the elements in spin-on dielectric CoTiO₃ with 600°C annealing. As shown in figure 3.6, it is obvious that carbon element signal only exists at the start of analysis, i.e. at surface. The surface carbon may be resulting form the absorption of residual in the air. Hence

there is no carbon element in the dielectric formed by this sol-gel spin coating method.

In this analysis, because we didn't have the reference sample to derive the relative sensitivity factor for evaluating atomic concentration in depth profile, there is an error in the atomic percentage in the figure 3.6. Despite this deviation, the qualitative composition result could be acceptable.

3.3.2 *Electron Spectroscopy for Chemical Analysis*

There is no doubt that the spin-on dielectrics only contains cobalt, titanium and oxygen elements, which is confirmed by EDS analysis in section 3.1 and Auger depth profile in section 3.1. However, we still don't know the chemical properties and atomic concentration ratio of this dielectric prepared by sol-gel spin coating. In the section we use electron spectroscopy for chemical analysis (ESCA) to obtain further information.

Figure 3.7 shows ESCA results of the dielectric formed by sol-gel spin coating method and the dielectric under analysis is 1-coated and annealed at 600°C. From figure 3.7(a) to 3.7(d) are the spectrums of silicon 2*p* orbital, oxygen 1*s* orbital, cobalt 2*p* orbital and titanium 2*p* orbital, respectively. As shown in figure 3.7(a), two main peaks identify single crystalline silicon (99.3 eV) and silicon dioxide (103.3 eV) in the silicon 2*p* orbital spectrum. We also observe that the shift and the growth of the silicon-dioxide-peak increases, as the annealing temperature is increased, which means that more complete structure and thicker silicon oxide are formed after higher temperature annealing. The spectrum of oxygen 1*s* orbital shown in figure 3.7(b) reveals that there may be two kinds of metal-oxygen bonds with lower binding energy near 531 eV , e.g. Co-O and Ti-O for all samples. However, the broader binding energy distribution for the sample annealed at 200°C may be resulting from hydroxides in the dielectric [27]. Furthermore, the samples with 800°C and 900°C

annealing have silicon oxide bond with binding energy near 533 eV, which is consistent with the results in figure 3.7(a). We also notice that two shake-up peaks with higher binding energy than two main peaks ($2p_{3/2}$ and $2p_{1/2}$) appear in the Co spectrum, as shown in figure 3.7(c).

In order to confirm the atomic concentration ratio of the dielectric prepared by sol-gel spin coating method, more detailed ESCA analysis for the spin-on dielectric annealed at 600 °C is executed. After background removal by Shirley method and curve fitting for oxygen-metal bonds (oblique line area) in oxygen spectra, we integrate the intensity from 775 to 810 eV for cobalt spectra, from 453 to 468 eV for titanium spectra and from 527 to 535 eV for oxygen spectra, as shown in figure 3.8. The relative sensitivity factors for cobalt, titanium and oxygen are 3.529, 2.077 and 0.733, respectively. And the atomic concentration ratio is obtained as,

$$[Co]:[Ti]:[O] = \frac{A_{Co}}{SF_{Co}} \cdot \frac{A_{Ti}}{SF_{Ti}} \cdot \frac{A_{O}}{SF_{O}} = \frac{93175.67}{3.529} \cdot \frac{53580.63}{2.077} \cdot \frac{53828.65}{0.733}$$

$$\approx 1:0.97:3.04.$$

Therefore, the atomic concentration ratio is almost close to 1:1:3.

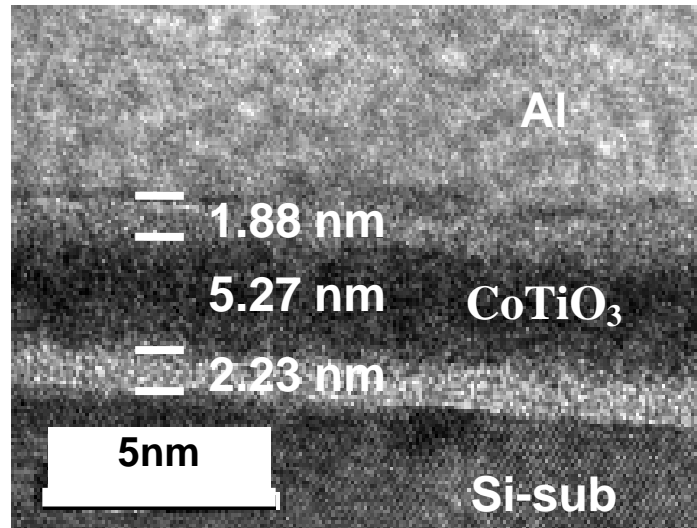


Fig. 3.1 TEM image of Al-electrode/1-coated CoTiO_3 thin film/bare Si structure.

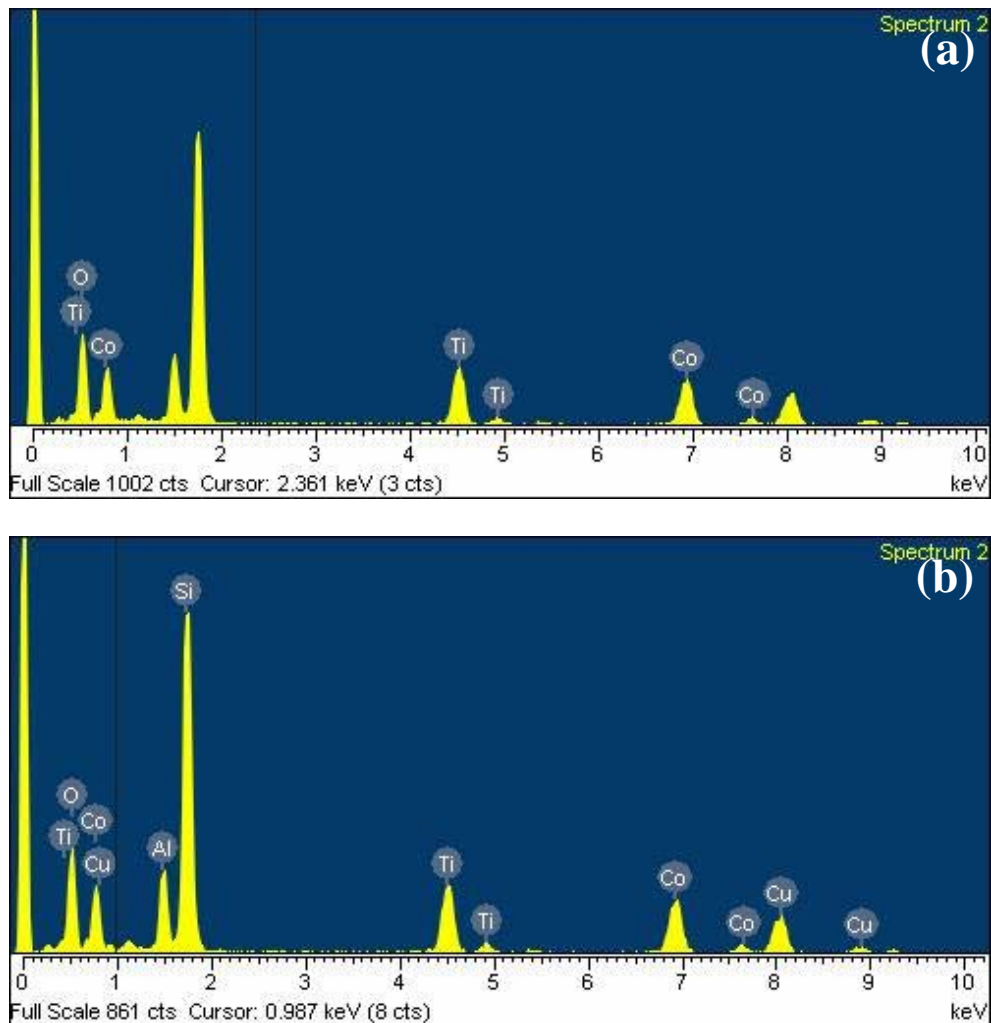


Fig. 3.2 Electron dispersive spectra (EDS), associated with the TEM image showed in Fig. 3.1, of the CoTiO_3 dielectric annealed at 400°C .

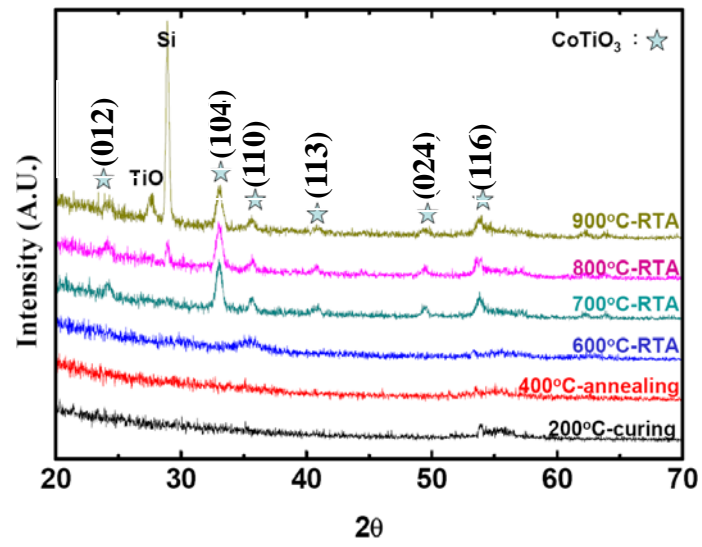
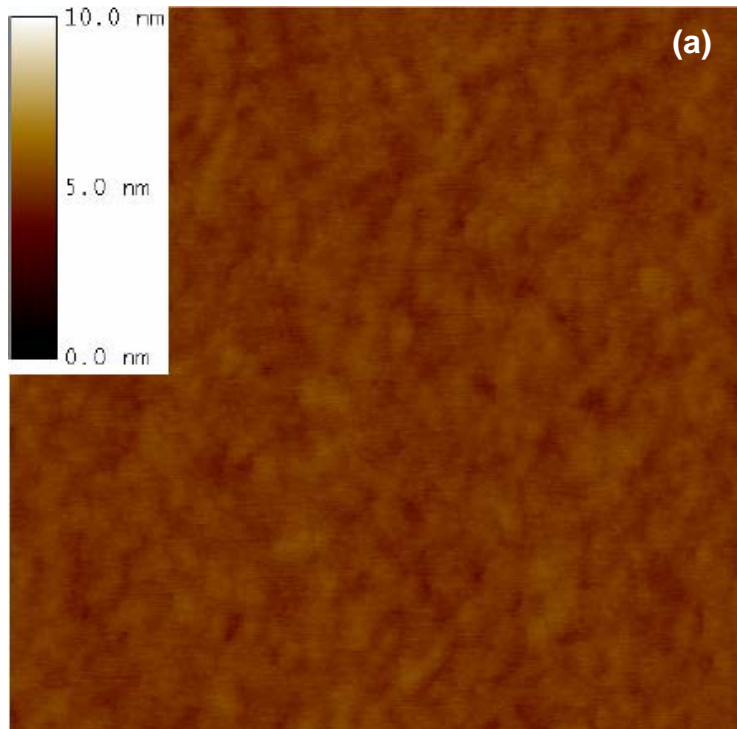
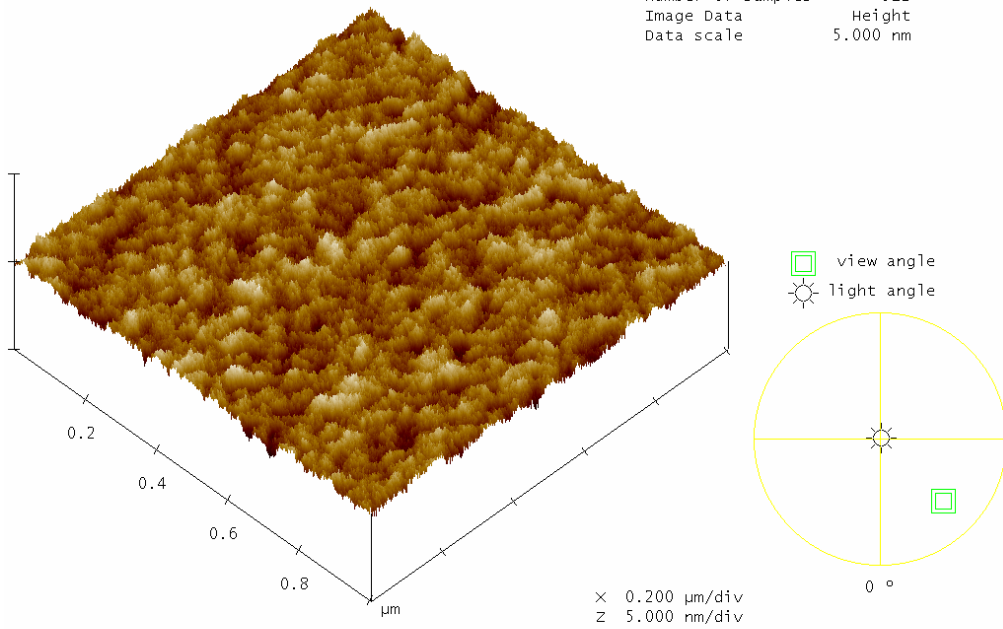


Fig. 3.3 XRD spectra of spin-on CoTiO_3 films. The marked peaks correspond to crystallized CoTiO_3 phases.

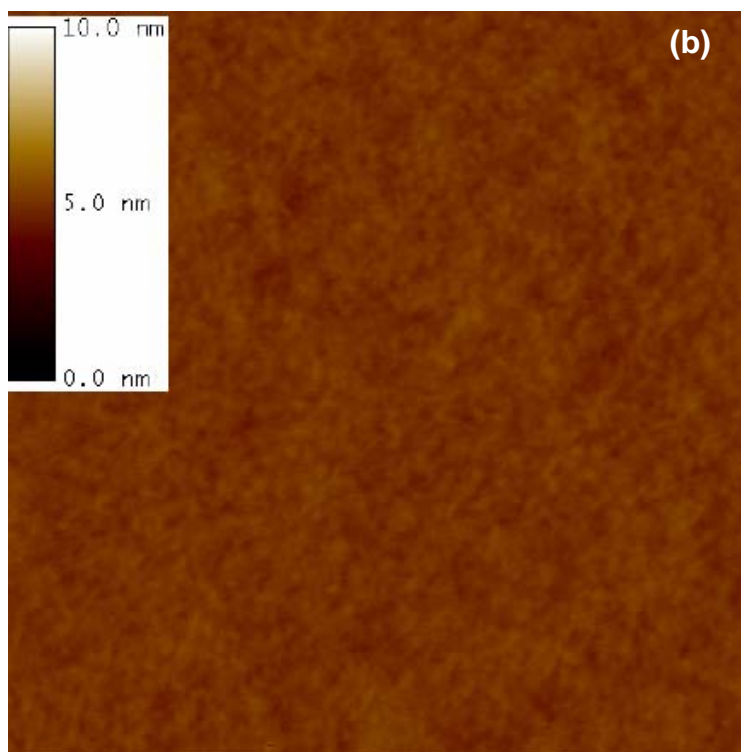




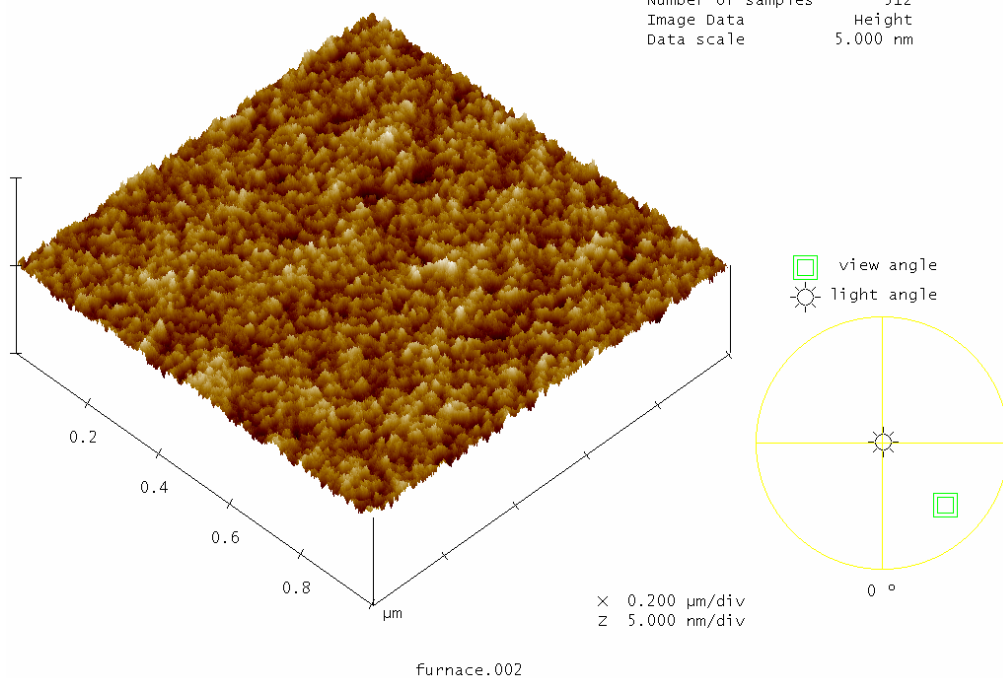
Digital Instruments NanoScope
 Scan size 1.000 μm
 Scan rate 0.7016 Hz
 Number of samples 512
 Image Data Height
 Data scale 5.000 nm

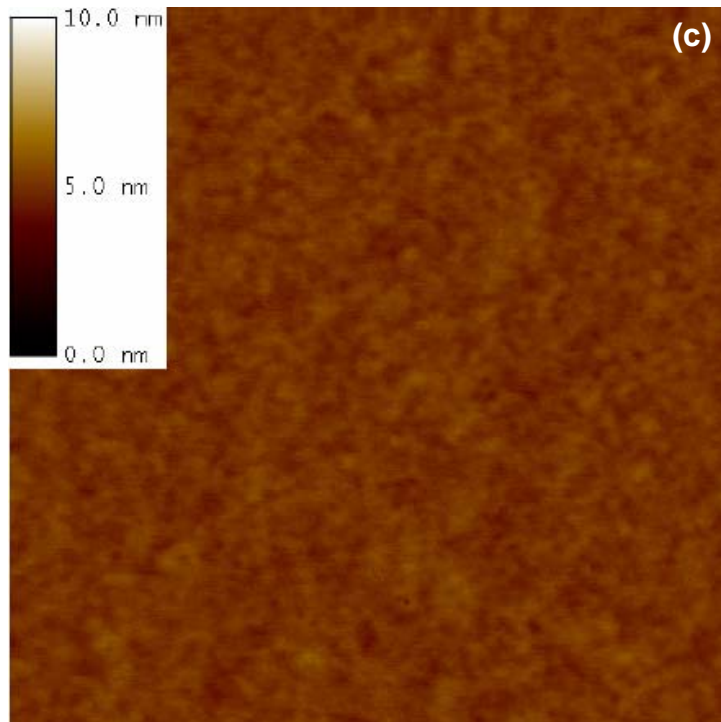


curing.003

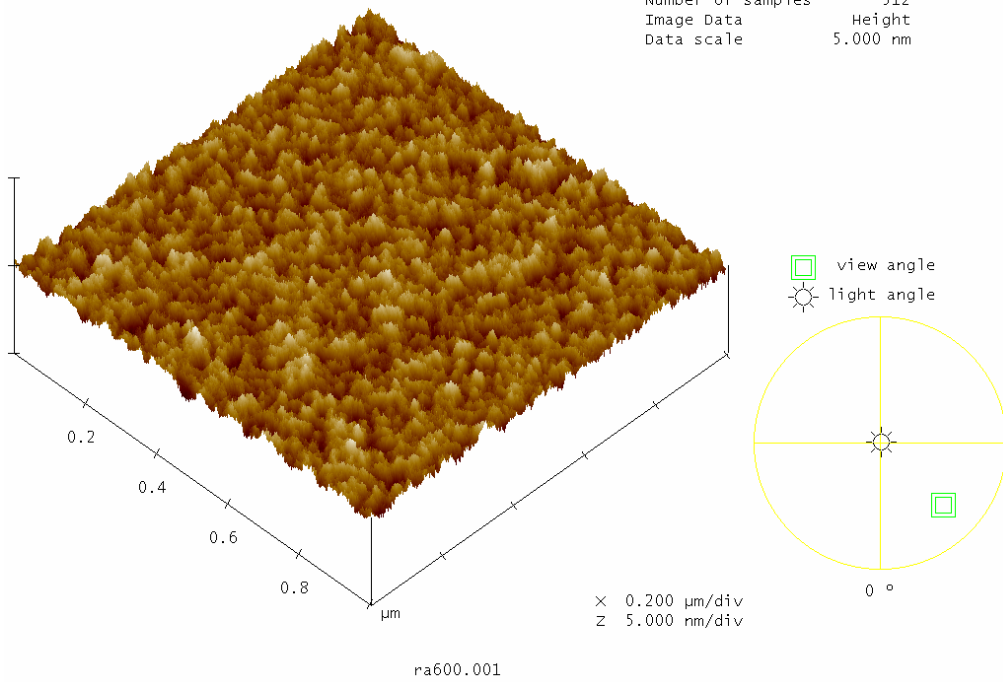


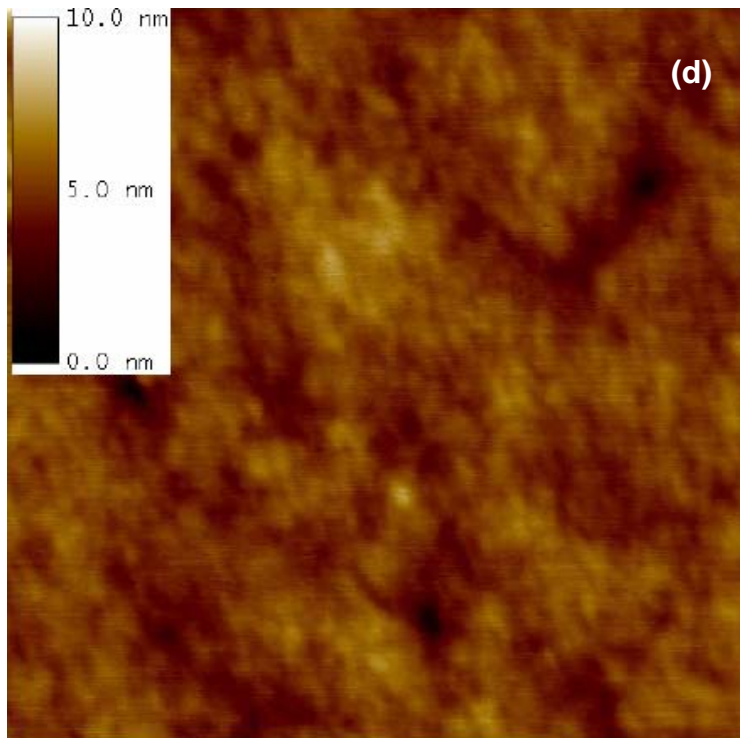
Digital Instruments NanoScope
 Scan size 1.000 μm
 Scan rate 0.7016 Hz
 Number of samples 512
 Image Data Height
 Data scale 5.000 nm



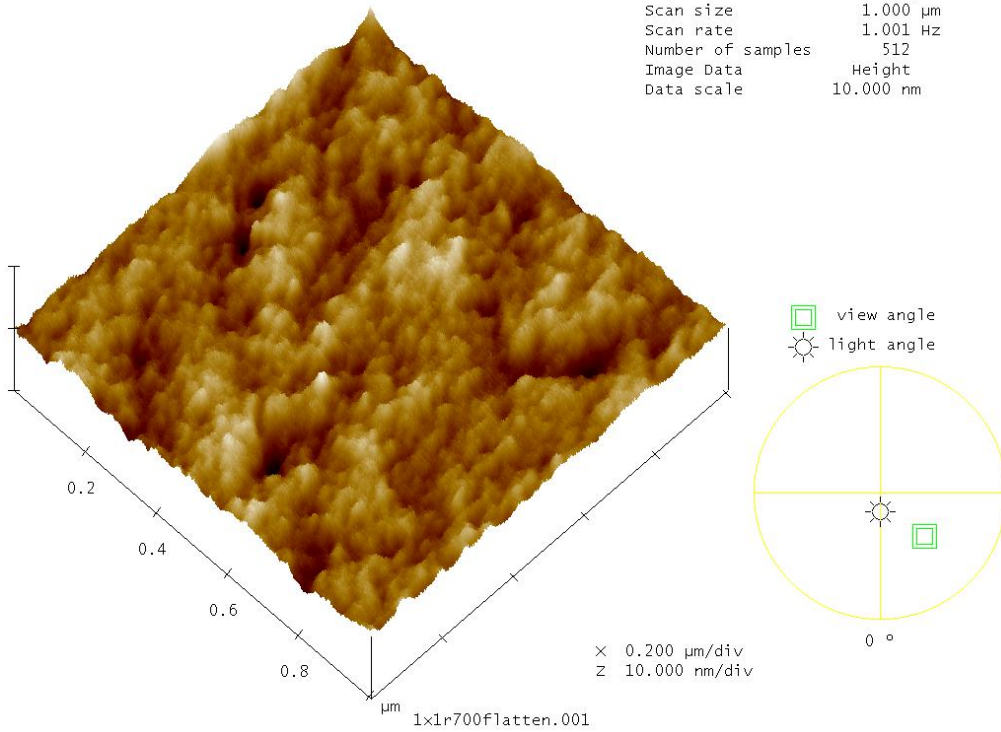


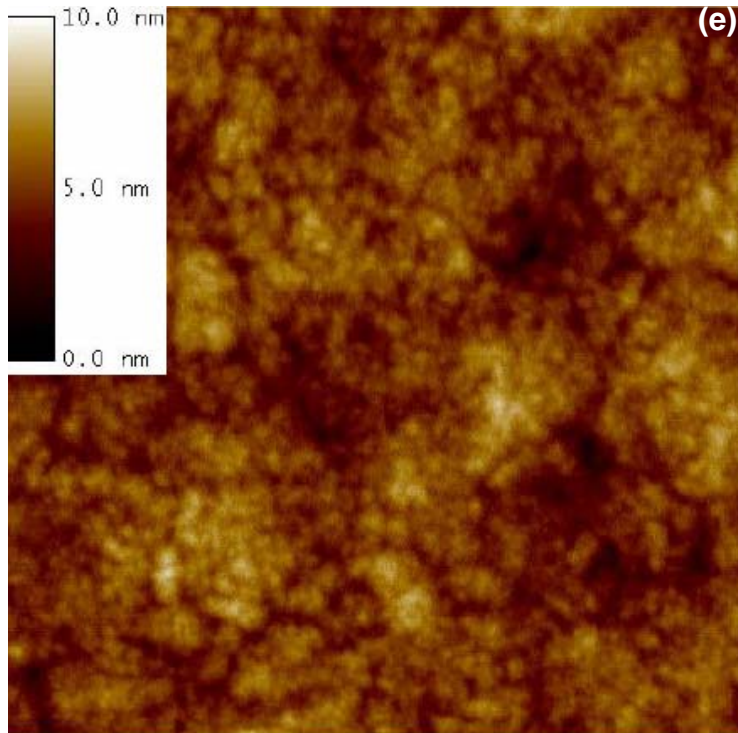
Digital Instruments NanoScope
 Scan size 1.000 μm
 Scan rate 0.7016 Hz
 Number of samples 512
 Image Data Height
 Data scale 5.000 nm



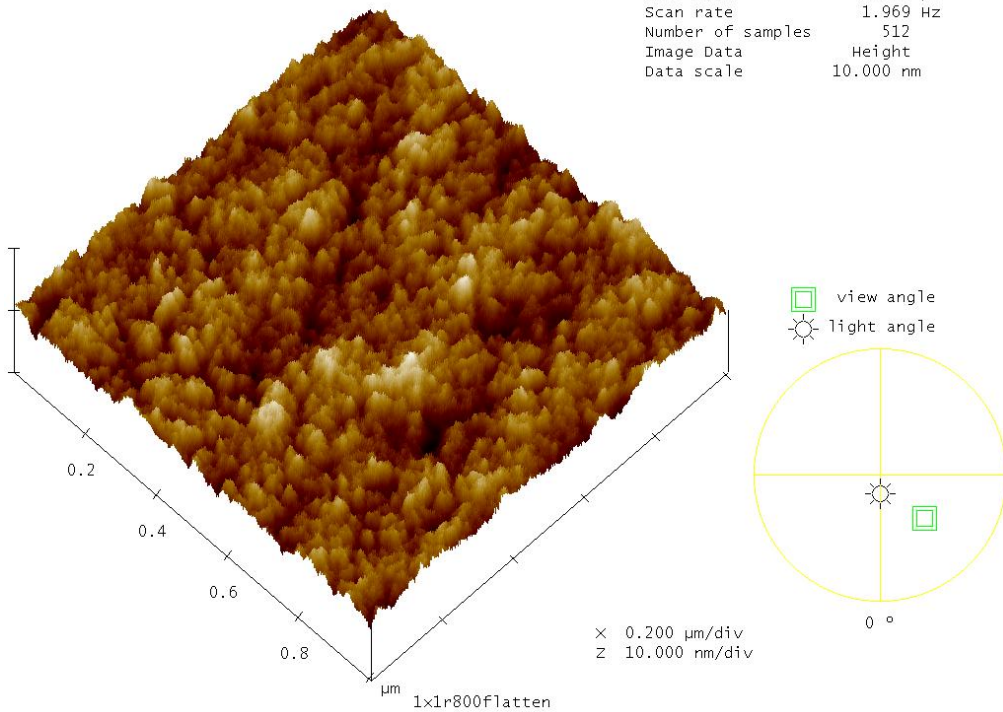


Digital Instruments NanoScope
 Scan size 1.000 μm
 Scan rate 1.001 Hz
 Number of samples 512
 Image Data Height
 Data scale 10.000 nm





Digital Instruments NanoScope
 Scan size 1.000 μm
 Scan rate 1.969 Hz
 Number of samples 512
 Image Data Height
 Data scale 10.000 nm



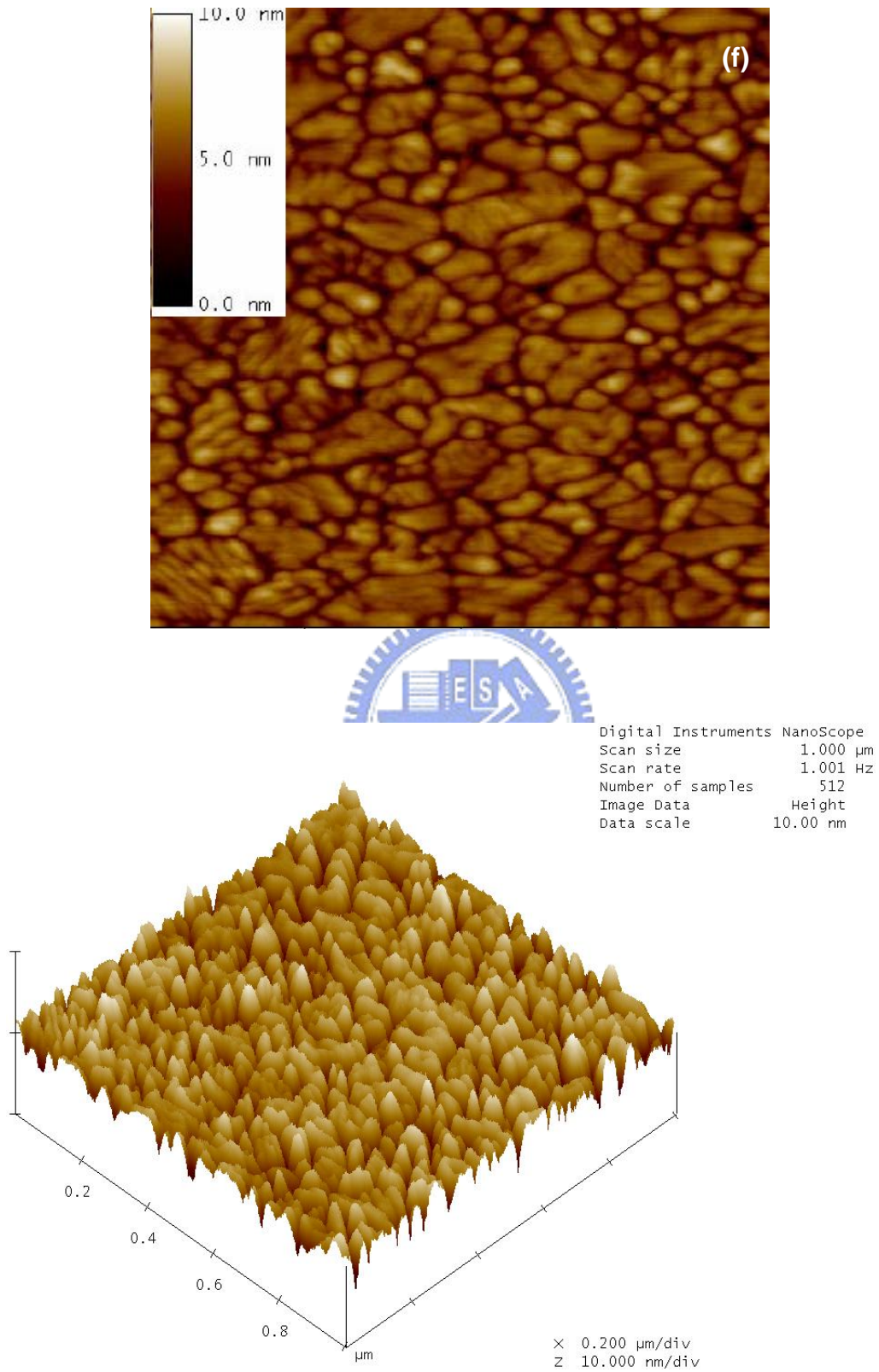


Fig. 3.4 SPM images of spin-on CoTiO_3 films with various thermal treatments at (a) 200°C , (b) 400°C , (c) 600°C , (d) 700°C , (e) 800°C and (f) 900°C . The image size is $1\ \mu\text{m}$ by $1\ \mu\text{m}$.

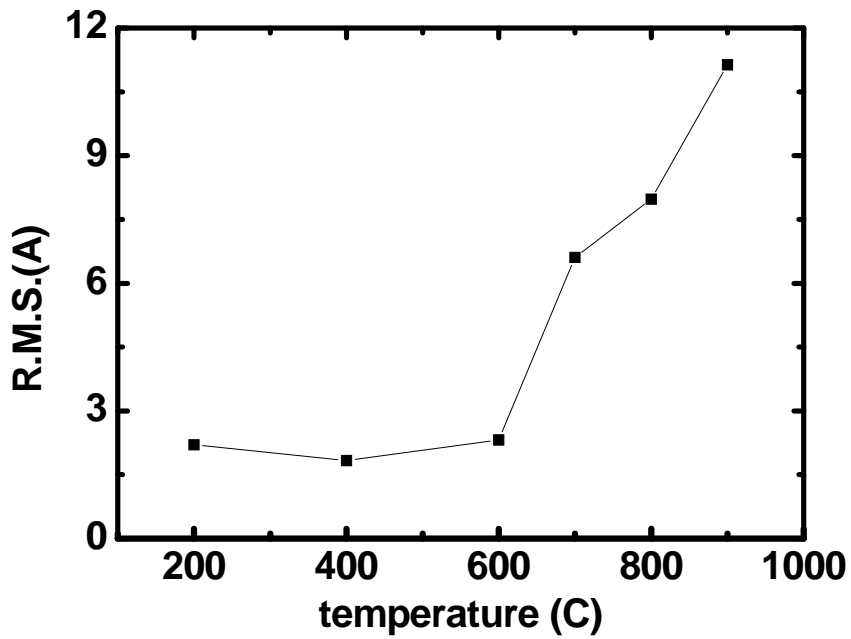


Fig. 3.5 Surface roughness of spin-on dielectrics as functions of annealing temperature.

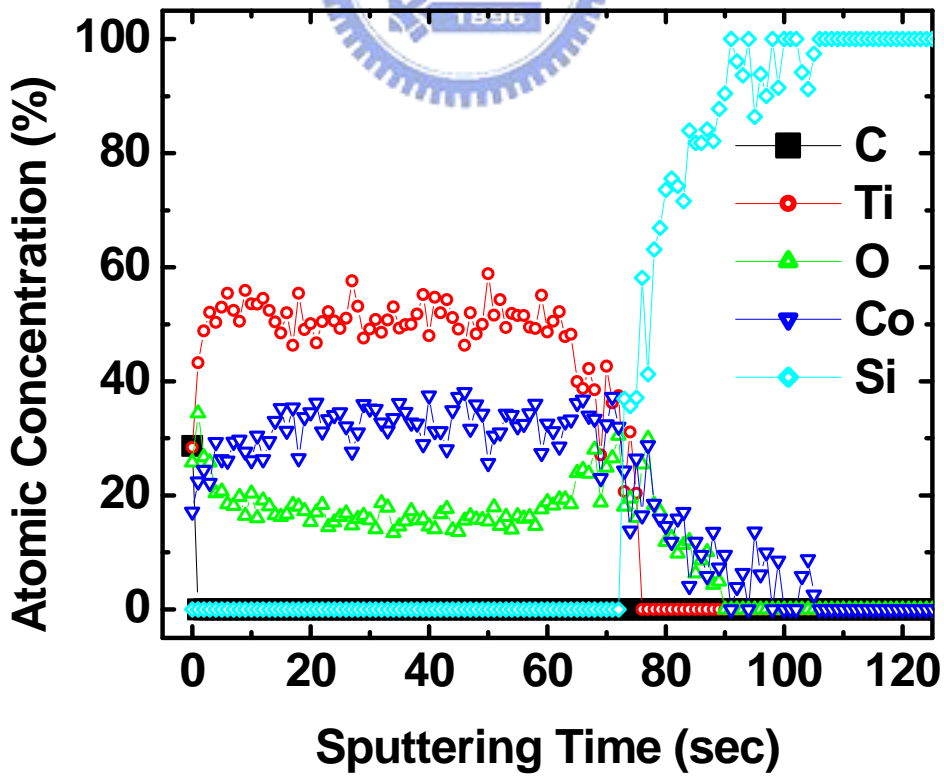


Fig. 3.6 Auger depth profile of the CoTiO₃ dielectric annealed at 600°C.

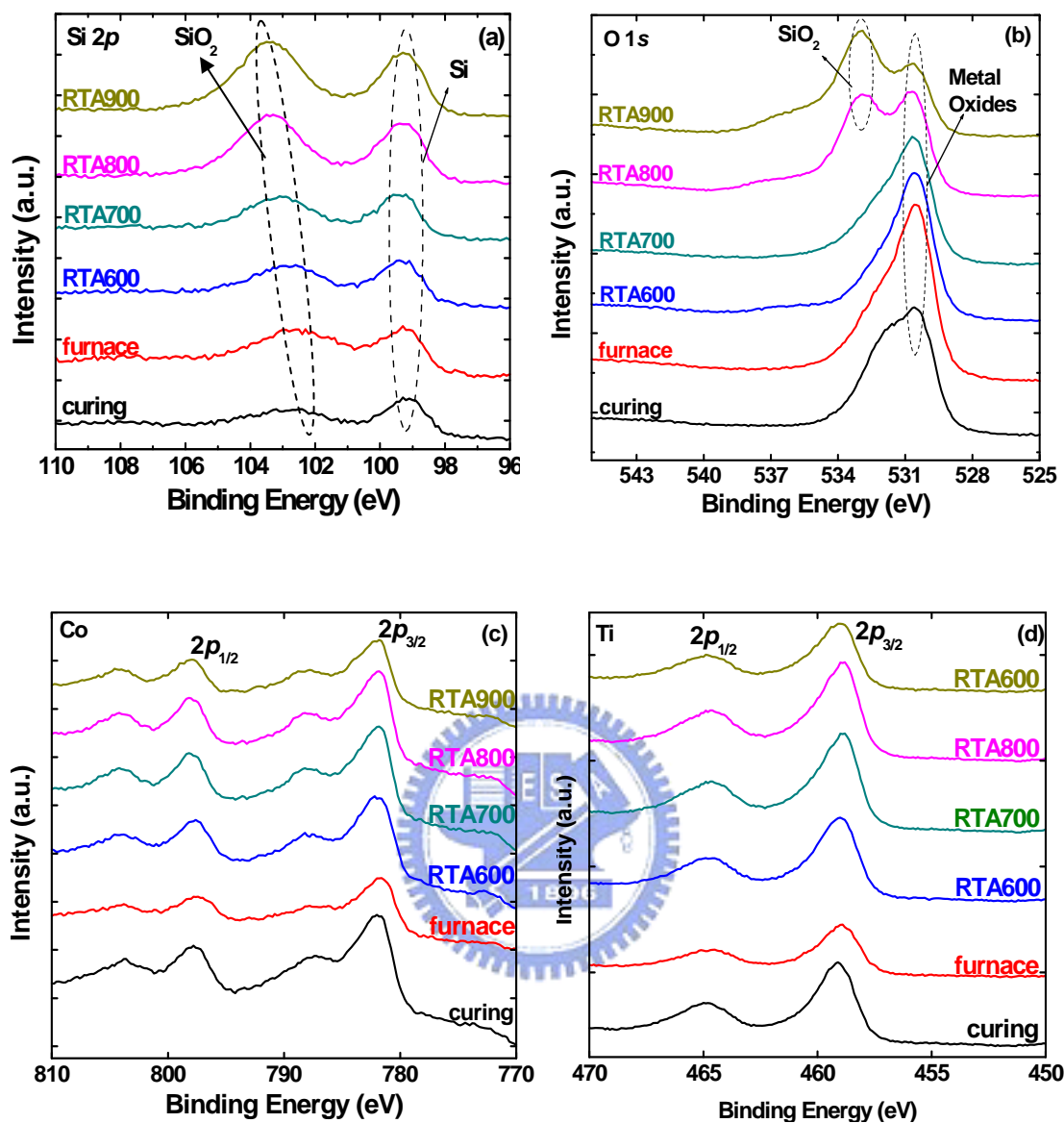


Fig. 3.7 ESCA spectra of Si 2p(a), O 1s(b), Co 2p(c) and Ti 2p(d) with different annealing temperature.

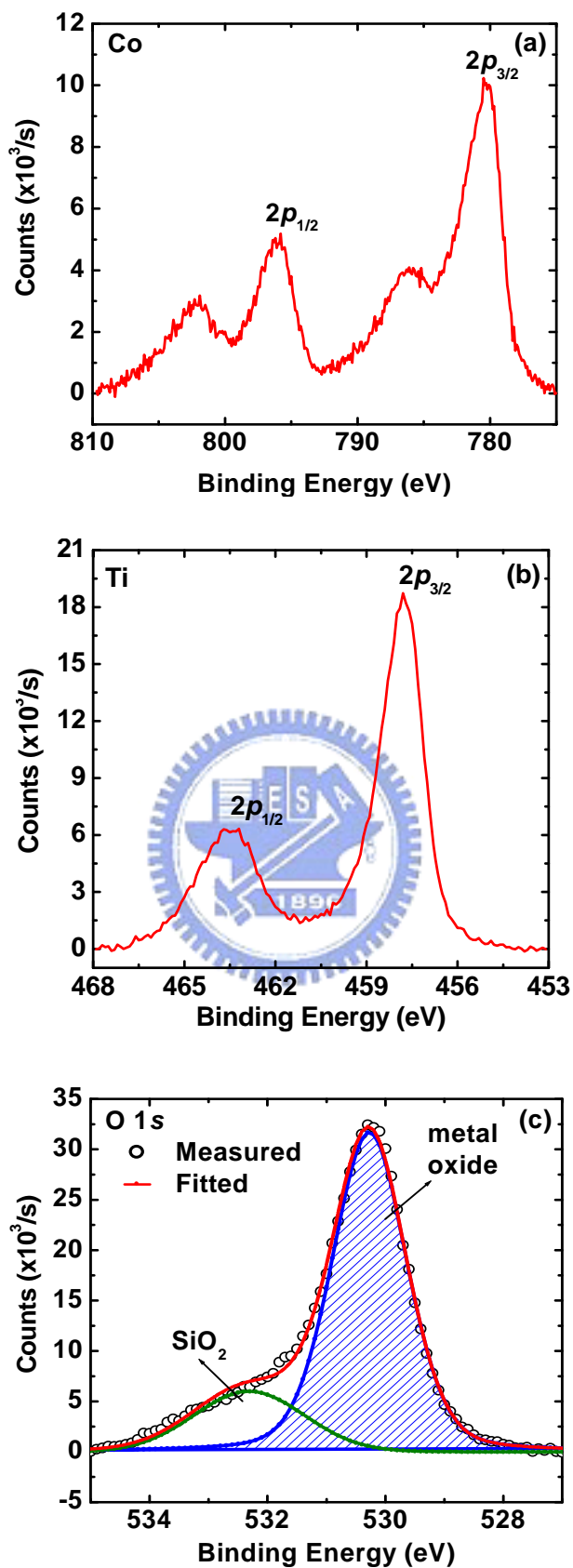


Fig. 3.8 ESCA spectra of Co 2p(a), Ti 2p(b) and O 1s(c) for the spin-on dielectric annealed at 600°C.

Chapter 4

Physical Property

In this chapter, we will report the physical properties of spin-on CoTiO₃ thin films, such as dielectric permittivity, C - V and I - V characteristics, current transport mechanism, band energy gap and band alignment.

4.1 Dielectric Permittivity

According to section 3.1.1, it is easy to form an interfacial layer between Si-sub and a CoTiO₃ film. However, it is imprecise and difficult to extract the κ value of CoTiO₃ film from measuring capacitance. In order to estimate the dielectric constant of CoTiO₃ thin films, a thermal oxidation is used to grow a high quality SiO₂ thin layer before the CoTiO₃ spin-coating. The C - V characteristics of both TaN/CoTiO₃/SiO₂/Si and TaN/SiO₂/Si capacitors are demonstrated in Fig. 4.1. The well C - V characteristics can be observed for both two capacitors without flat-band voltage shift, as shown in Fig. 4.1. The capacitance effective thickness (CET) is extracted from C - V curves at 100 kHz without considering quantum effect. The CET of CoTiO₃/SiO₂ and SiO₂ are 4.66nm and 4.27nm, respectively. However figure 4.2 shows HR-TEM image of the Si/SiO₂/CoTiO₃/TaN structure. Thicknesses of 1-coated high- k dielectric and thermal oxide are 4.02 and 4.27 nm, respectively, as shown in this TEM image. As a result, the exact dielectric constant of CoTiO₃ thin film is found to be 40.2, which is matched the value of CoTiO₃ films fabricated by direct oxidation of sputtered Co/Ti layers [28][29], indicating that the high permittivity CoTiO₃ films can also be deposited by simple sol-gel spin coating method.

4.2 C - V and I - V Characteristics

Figure 4.3 shows the C - V characteristics of CoTiO₃ gate dielectric with different

thermal treatments. The sample with 600°C RTA shows a steeper $C-V$ slope in the depletion region, suggesting a better CoTiO_3/Si interface. RTA temperatures beyond 600°C result into flatter $C-V$ curves which may be due to the sub-stoichiometric interfacial-oxide growth and thermal stress.

Figure 4.4 shows the $I-V$ characteristics of CoTiO_3 gate dielectrics. The leakage current density increases with increasing RTA temperature (600~900°C), even though the $C-V$ curves suggest a larger effective oxide thickness (EOT) for samples annealed at higher temperatures. This can be explained by the cracks and crystallization of CoTiO_3 thin films, as discussed before. Finally we sum up the fundamental electrical behavior of spin-on CoTiO_3 dielectric in figure 4.5, and the dielectric annealed at 600°C has the smallest EOT.

4.3 *Current Transport Mechanism*

Figure 4.6 shows the $I-V$ curves measured at elevated temperatures. The CoTiO_3 film under test was annealed at 600°C. The $I-V$ curves were fitted by the Schottky emission model (inset), and the barrier heights of 0.74, 0.72, 0.70, and 0.69eV were extracted at room temperature, 40°C, 50°C, and 60°C, respectively. Fittings with the Frenkel-Poole (FP) conduction model were also carried out. Figure 4.7 demonstrates that the current conduction is not dominated by the FP conduction but by the Schottky emission, which shows a smaller Si/CoTiO_3 barrier height.

4.4 *Band Energy gap and Band Alignment*

As mentioned in Section 1.5, XPS technique can be utilized to determine the band gap energy. In this section we characterize the band gaps of SiO_2 and the spin-on CoTiO_3 dielectric annealed at 600°C. In order to align the band diagram, we also use high resolution XPS analyzer to detect the maximum valence energy band level of

thermally grown SiO₂ and the spin-on CoTiO₃ dielectric [30].

As mentioned in Section 1.5, the background rise below XPS core level peaks is due to inelastic scattering effects of the photon-electrons. More importantly, the excitation of the electrons from valence band to conduction band can also be detected at the onset of plasma energy loss. As a result, the onset of the background increase relative to the peak position corresponds with the band gap of the material. Figure 4.8 shows the spectrum of oxygen 1s orbital for SiO₂, which is illustrating that the energy band gap of thermal SiO₂ is about 9.0 eV. This value is almost close to the common results [6][7]. Furthermore, the high resolution core level and band gap spectra of spin-on CoTiO₃ film is shown in Fig. 4.9. The energy band gap of spin-on CoTiO₃ is about 2.2 eV, which is close to the value of CoTiO₃ powders fabricated by a modified Pechini method [31].

On the other hand, the measurements are performed on thermal SiO₂ (~15nm) and the 5-coated dielectric CoTiO₃ (~20nm)/SiO₂ (~15nm) stacks. The valance band spectrum for these layers contains the information about the density of states of both the CoTiO₃ and SiO₂ films. The maximum valence energy band and the valence band offset (ΔE_v) between CoTiO₃ and SiO₂ films can thus be determined as about 4.0 eV, as indicated in Fig. 4.10.

As mention in figure 4.7, the energy barrier height between silicon substrate and spin-on CoTiO₃ dielectric is about 0.74 eV at room temperature. Because the energy band alignment between Si and SiO₂ is a well-known result, we can deduce the band alignment between Si, SiO₂ and spin-on CoTiO₃ dielectric, as shown in figure 4.11. Figure 4.11 shows the energy band alignment between Si, SiO₂ and high-*k* dielectric CoTiO₃, which serves to summarize the key results we have obtained from the analysis of HR-XPS and Schottky emission characteristics. And this deduction is consistent with the result in figure 4.9.

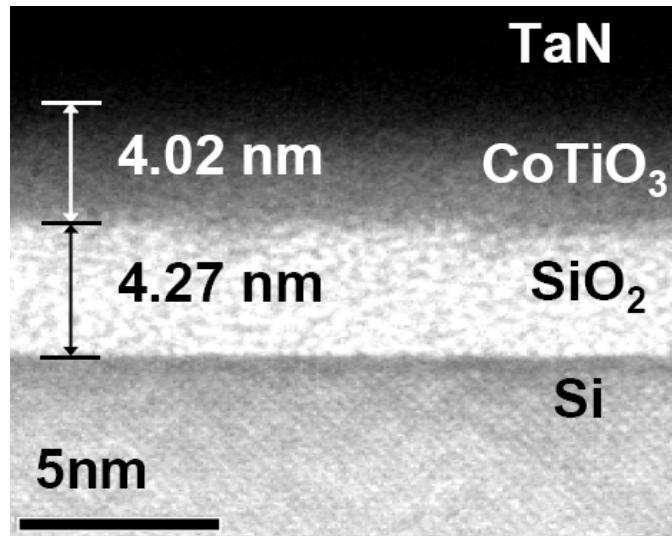


Fig. 4.1 TEM micrograph of an ultrathin CoTiO_3 film spin-coated on a high quality thermal SiO_2 layer and annealed at 600°C .

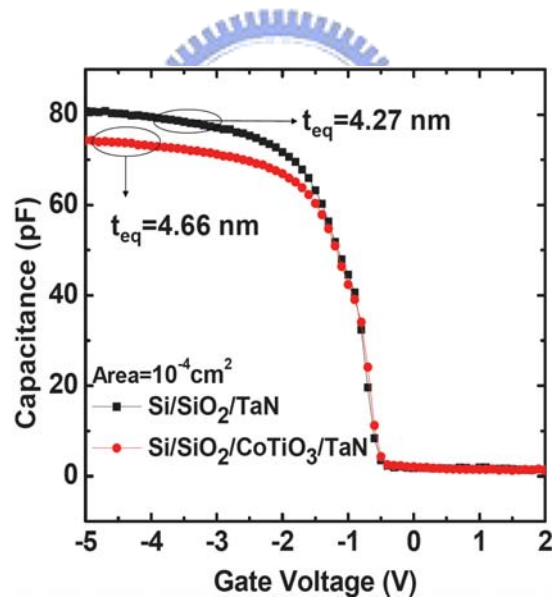


Fig. 4.2 C - V curves of capacitors with $\text{TaN}/\text{CoTiO}_3/\text{SiO}_2/\text{Si}$ and $\text{TaN}/\text{SiO}_2/\text{Si}$ stack structures.

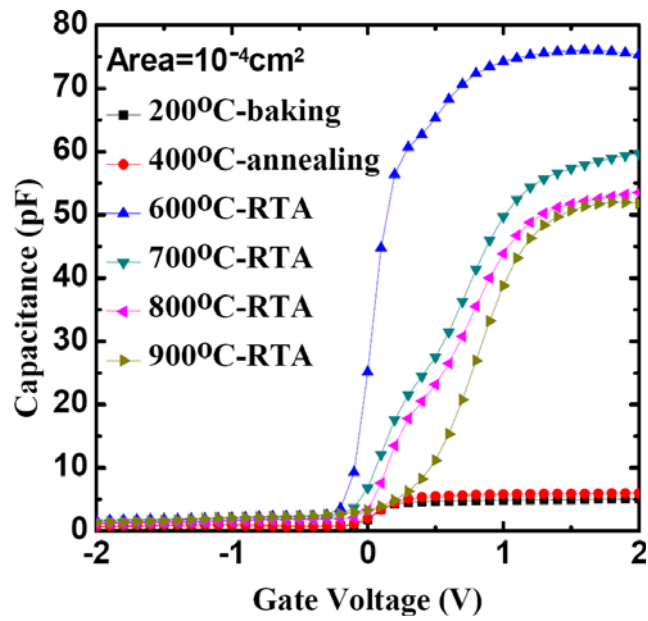


Fig. 4.3 C - V curves of spin-on CoTiO_3 films with different thermal treatments.

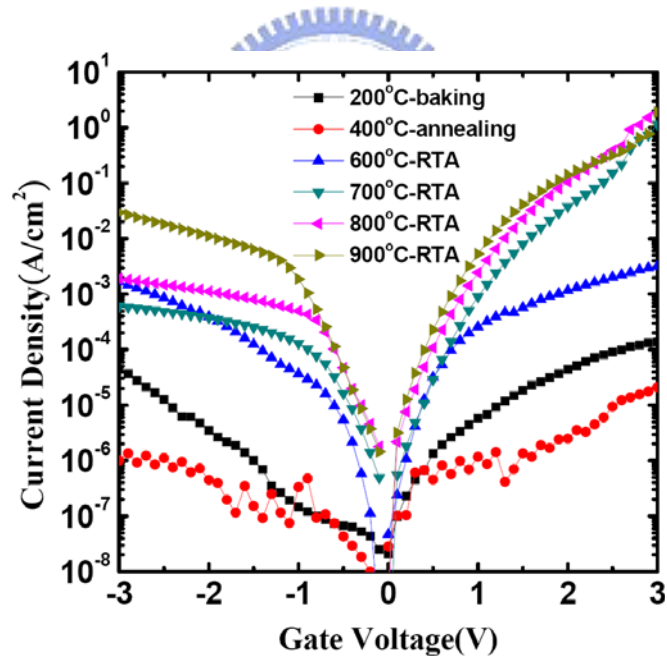


Fig. 4.4 I - V curves of spin-on CoTiO_3 films with different thermal treatments.

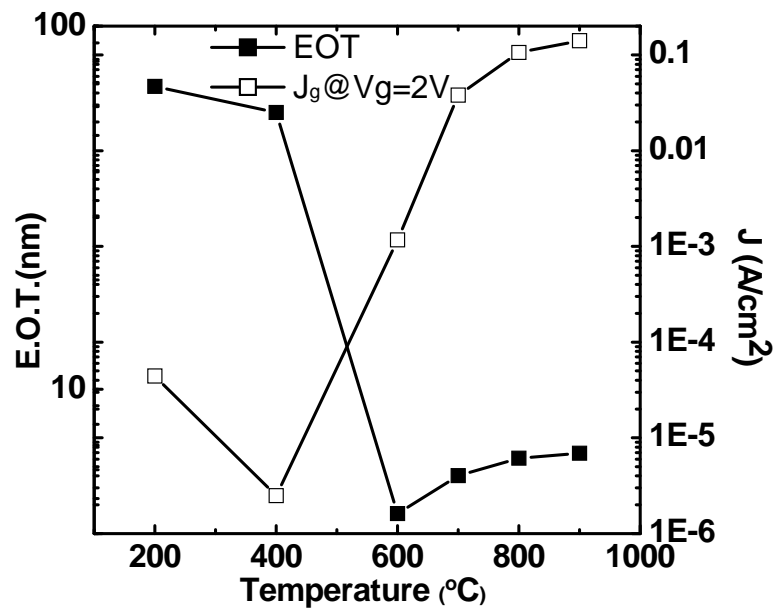


Fig. 4.5 Effective oxide thickness and current density of spin-on dielectrics as functions of annealing temperature.



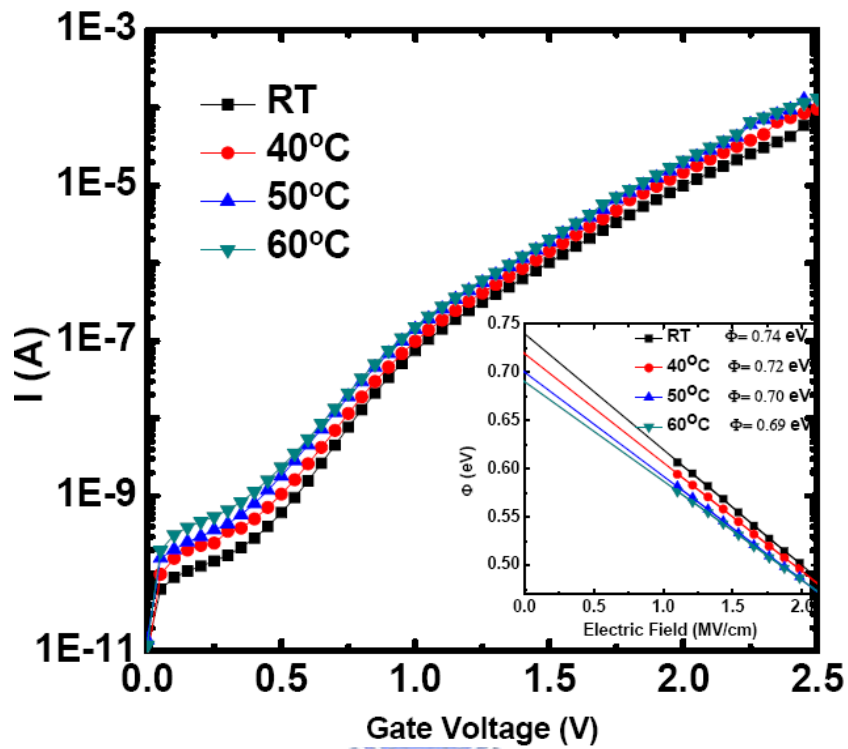


Fig. 4.6 I - V curves measured at RT and elevated temperatures. (Inset) Extracted Schottky-emission barrier heights.

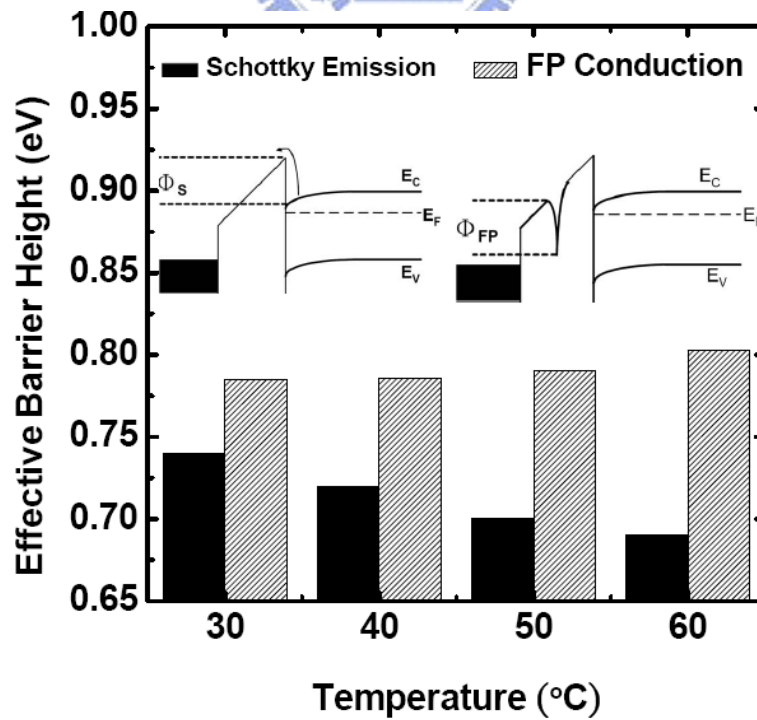


Fig. 4.7 Effective barrier heights extracted from I - V curves by using Schottky-emission and Frenkel-Poole models.

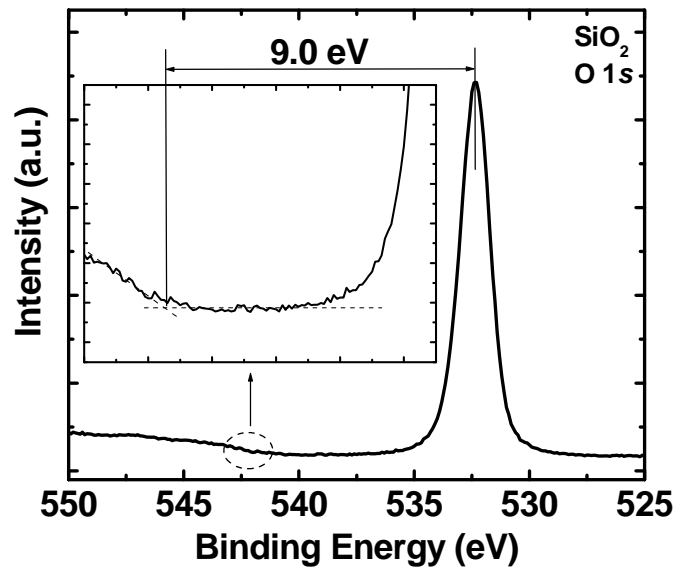


Fig. 4.8 ESCA spectra of O 1s for thermally grown 15 nm-SiO₂.

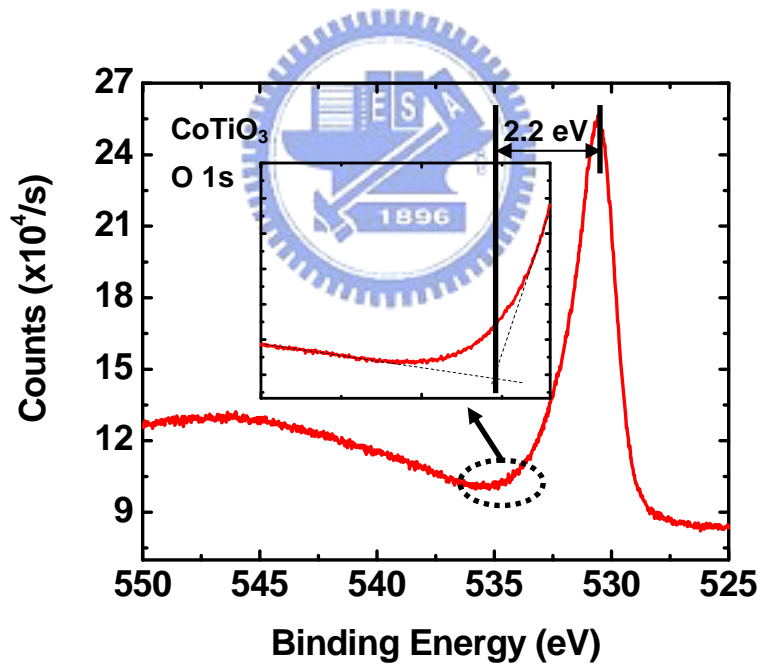


Fig. 4.9 ESCA spectra of O 1s for the spin-on 15 nm-CoTiO₃ dielectric annealed at 600°C.

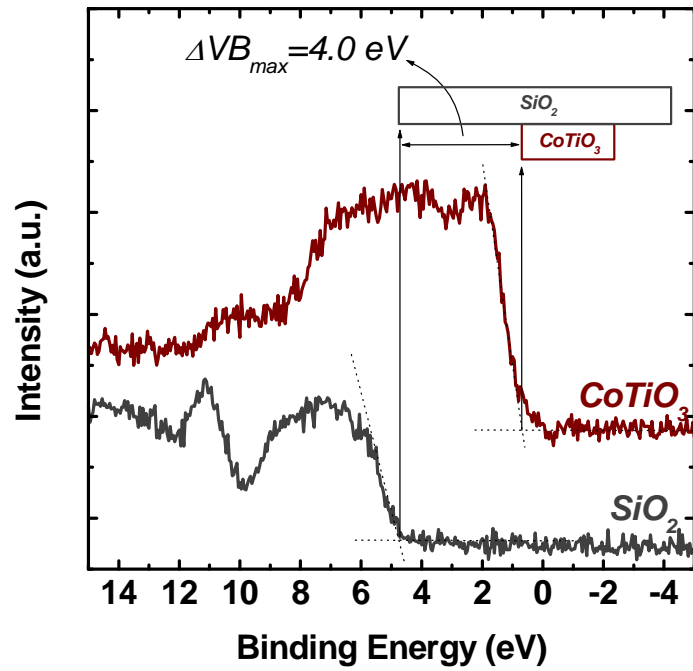


Fig. 4.10 Maximum valence energy band spectra of thermally grown 15 nm-SiO₂ and spin-on 20 nm CoTiO₃ dielectric annealed at 600°C measured by high resolution ESCA.

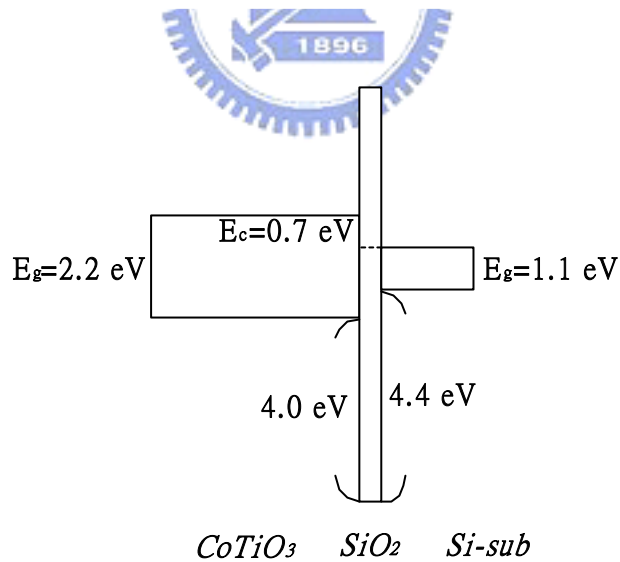


Fig. 4.11 Band alignment between Si, SiO₂ and spin-on CoTiO₃ dielectric with 600°C annealing.

Chapter 5

Conclusions

In this chapter we will summarize the important results of spin-on CoTiO_3 as mentioned in previous chapters and make conclusions for this these.

5.1 Conclusions

In this thesis we form the dielectric CoTiO_3 by sol-gel spin coating method followed by different annealing temperature 600~900°C. The image of transmission electron microscopy (TEM), as shown in Fig. 3.1, reveals that 2.2 nm interfacial layer is between Si-sub and CoTiO_3 with 400°C annealing. According to X-ray diffraction (XRD) pattern in Fig. 3.3, crystallization temperature of the spin-on dielectric is between 600 and 700°C. As shown in Fig. 3.4 and Fig. 3.5, scanning probe microscope (SPM) describes surface morphology of the spin-on dielectrics with different annealing temperature and the surface roughness abruptly increases as annealing temperature higher than 600 °C. Electron spectroscopy for chemical analysis (ESCA) in Fig. 3.7 shows that higher temperature annealing results in thicker interfacial layer and pure chemical bonding. Furthermore ESCA in Fig. 3.8 also confirms that the spin-on dielectric with 600°C annealing has atomic concentration ratio $[\text{Co}]:[\text{Ti}]:[\text{O}] \sim 1:1:3$. The spin-on film CoTiO_3 with 600°C annealing has Schottky emission conduction mechanism for the TaN/ CoTiO_3 / Si-sub structure and the evidences are presented in Fig. 4.6 and Fig.4.7. And the trapping characteristics of spin-on film CoTiO_3 with 600°C annealing is affected by temperature, applied stress voltage and stress time.

High electrical permittivity ($k \sim 40.2$) of CoTiO_3 dielectric is extracted via the high resolution transmission electron microscopy (HR-TEM) image and $C-V$ curves, as shown in Fig 4.1 and Fig. 4.2. In addition, the band energy gaps of thermally

grown SiO_2 and spin-on CoTiO_3 are 9.0 and 2.2 eV, respectively, as shown in Fig. 4.8 and Fig. 4.9. The valence energy band offset between thermally grown SiO_2 and spin-on CoTiO_3 is about 4.0eV, which is detected by high resolution X-ray photoelectron spectroscopy (HR-XPS) in Fig. 4.10. The energy band alignment of spin-on CoTiO_3 directly with SiO_2 and indirectly with Si is successfully determined in this thesis, as shown in Fig. 4.11.



Reference

- [1] B. G. Streetman and S. Banerjee, Solid State Electronic Device, 5th ed.: Prentice Hall Inc., 2000.
- [2] S.-H. Lo, D. A. Buchanan, Y. Taur, and W. Wang, "Quantum-Mechanical Modeling of Electron Tunneling Current from the Inversion Layer of Ultra-Thin-Oxide nMOSFET's," Electron Device Letters, IEEE, vol. 18, pp. 209-211, 1997.
- [3] S. O. Kasap, Principles of Electrical Engineering Materials and Devices: McGraw-Hill, 2002.
- [4] K. Eisenbeiser, J. M. Finder, Z. Yu, J. Ramdani, J. A. Curless, J. A. Hallmark, R. Droopad, W. J. Ooms, L. Salem, S. Bradshaw, and C. D. Overgaard, "Field effect transistors with SrTiO₃ gate dielectric on Si," Applied Physics Letters, vol. 76, pp. 1324-1326, 2000.
- [5] G. Lucovsky and B. Rayner, "Microscopic Model for Enhanced Dielectric Constants in Low Concentration SiO₂-Rich Noncrystalline Zr and Hf Silicate Alloys," Appl. Phys. Lett., vol. 77, pp. 2912, 2000.
- [6] S. M. Sze, Physics of Semiconductor Devices, 1985.
- [7] G. D. Wilk, R. M. Wallace, and J. M. Anthony, "High-k Gate Dielectrics: Current Status and Materials Properties Considerations," *J. Appl. Phys.*, vol. 89, pp. 5243, 2001.
- [8] G. D. Wilk and R. M. Wallace, *Appl. Phys. Lett.*, vol. 74, pp. 2854, 1999.
- [9] G. Lucovsky, Y. Wu, H. Niimi, V. Misra, and J. C. Phillips, *Appl. Phys. Lett.*, vol. 74, pp. 2005, 1999.
- [10] A. Kumar, D. Rajdev, and D. L. Douglass, *J. Am. Chem. Soc.*, vol. 55, pp. 439, 1972.
- [11] R. Chandrasekharan, Inkyu Park, R. I. Masel, and M. A. Shannon, "Thermal Oxidation of Tantalum Films at Various Oxidation States from 300 to 700 °C," *J. Appl. Phys.*, vol. 98, pp. 114908, 2005.
- [12] I. C. Kizilyalli, R. Y. S. Huang, P. K. Roy, "MOS Transistors with Stacked SiO₂ –Ta₂O₅ –SiO₂ Gate Dielectrics for Giga-Scale Integration of CMOS Technologies," Electron Device Letters, IEEE, vol. 19, pp. 423-425, 1998.
- [13] D. G. Park, H. J. Cho, et al. (2000). Tech. Dig. VLSI Symp.
- [14] J. H. Lee, K. Koh, et al. (2000). Tech. Dig. Int. Electron Devices Meet.
- [15] *The International Technology Roadmap for Semiconductors*, Semiconductor Industry Association.
- [16] J. C. Wang, D. C. Shie, et al. (2004). *Appl. Phys. Lett.* **84**: 1531.

- [17] Kuo-Hsing Kao, Jian-Hao Chen, et al. (2007). Characterization of CoTiO₃ Thin Films Formed by Sol-Gel Spin Coating with High Temperature Annealing. SNTD, Taiwan.
- [18] Hsin-Chiang You, Tze-Hsiang Hsu, et al. (2006). "Hafnium Silicate Nanocrystal Memory Using Sol-Gel-Spin-Coating Method." *Electron Device Letters*, IEEE **27**: 644.
- [19] Ko, F.-H., Hsin-Chiang You, et al. (2007). "Fabrication of SONOS-Type Flash Memory with the Binary High-k Dielectrics by the Sol-Gel Spin Coating Method." *Journal of The Electrochemical Society* **154**.
- [20] J. Tang, J. Fabbri, et al. (2004). *Chem. Mater* **16**: 1336.
- [21] L.C. Feldman and J.W. Mayer, *Fundamentals of Surface and Thin Film Analysis*, Elsevier Science Publishing Co., Inc., 1986.
- [22] D.A. Shirley, *Photoemission in Solids I*, Vol. 26 of *Topics in Applied Physics*, edited by M. Cardona and L. Ley (Springer-Verlag, Berlin, 1978), p.165.
- [23] S. Miyazaki, H. Nishimura, M. Fukuda, L. Ley, and J. Ristein, *Appl. Sur. Sci.* 113/114, 585-589 (1997).
- [24] J.L. Alay and M. Hirose, *J. Appl. Phys.*, 81, 1606, (1997).
- [25] H. Itokawa, T. Maruyama, S. Miyazaki, and M. Hirose, *Extended abstracts of the 1999 Int. Conf. Solid State Devices and Materials*, Tokyo, 1999, p. 158.
- [26] Hyeong Joon Kim, Qingyi Shao, Yoon-Hae Kim. *Surface and Coatings Technology*, 171 (2003), 39-45.
- [27] John F. Moulder, William F. Stickle, Peter E. Sobol, Kenneth D. Bomben, *Handbook of X-ray Photoelectron Spectroscopy*, Perkin-Elmer Corporation, 1992
- [28] T. M. Pan, et al *Appl. Phys. Lett.* 78, (2001) 1439
- [29] J. H. Chen, et al *J. Electrochem. Soc.*, 154, (2007)
- [30] F.G. Bell and L. Ley, *Phys. Rev. B*, 37, p.8383, (1988).
- [31] Yi-Jing Lin, Yen-Hwei-Chang, et al. (2005). "Synthesis and Characterization of Ilmenite NiTiO₃ and CoTiO₃ Prepared by a Modified Pechini Method." *Journal of Non-Crystalline Solid*, 352 789-794.
- [32] K. Kukli, et al *J. Appl. Phys.* 92, 5698 (2002).
- [33] C. M. perkins, et al *Appl. Phys. Lett.* 78, 2357 (2001).

Publication List

A. International Journal Paper :

- [A-1] Ming-Wen Ma, Tien-Sheng Chao, **Kuo-Hsing Kao**, Jyun-Siang Huang, and Tan-Fu Lei, "Fringing electric field effect on 65-nm-node fully depleted silicon-on-insulator devices," *Japanese Journal of Applied Physics*, vol. 45, no. 9A, pp.6854-6859, 2006.
- [A-2] Ming-Wen Ma, Chin-Yang Chen, Chun-Jung Su, Woei-Cherng Wu, **Kuo-Hsing Kao**, Tien-Sheng Chao, and Tan-Fu Lei, "Reliability mechanisms of LTPS-TFT with HfO₂ gate dielectric: PBTI, NBTI and hot carrier stress," *IEEE Trans. Electron Devices*, have been accepted for publication.
- [A-3] Ming-Wen Ma, Chin-Yang Chen, Chun-Jung Su, Woei-Cherng Wu, Tsung-Yu Yang, **Kuo-Hsing Kao**, Tien-Sheng Chao, and Tan-Fu Lei, "Improvement on performance and reliability of TaN/HfO₂ LTPS-TFTs with fluorine implantation," *Solid State Electronics*, vol. 52, no. 3, pp.342-247, 2008.

B. International Letter Paper :

- [B-1] **Kuo-Hsing Kao**, Shiow-Huey Chuang, Jian-Hao Chen, Ming-Wen Ma, and Tien-Sheng Chao, "High resolution XPS energy band alignment of CoTiO₃ high- k dielectric prepared by sol-gel spin coating method," *Applied Physics Lett.*, in revision.
- [B-2] Ming-Wen Ma, Yi-Hong Wu, **Kuo-Hsing Kao**, Woei-Cherng Wu, Tien-Sheng Chao, and Tan-Fu Lei, "Impacts of N₂ and NH₃ plasma surface-treatment on high performance LTPS-TFT with high- κ gate dielectric," *IEEE Electron Device Lett.*, in version.
- [B-3] Ming-Wen Ma, Tien-Sheng Chao, **Kuo-Hsing Kao**, Jyun-Siang Huang, and Tan-Fu Lei, "High- κ material sidewall with source/drain-to-gate non-overlapped structure for low standby power applications," *Japanese Journal of Applied Physics*, vol. 45, no. 11, pp.8656-8658, 2006.
- [B-4] Ming-Wen Ma, Chien-Hung Wu, Tsung-Yu Yang, **Kuo-Hsing Kao**, Woei-Cherng Wu, Tien-Sheng Chao, and Tan-Fu Lei, "Impact of high- κ offset spacer in 65-nm node SOI devices," *IEEE Electron Device Lett.*, vol. 28, no. 3, pp.238-241, March, 2007.
- [B-5] Ming-Wen Ma, Tien-Sheng Chao, Chun-Jung Su, Woei-Cherng Wu, **Kuo-Hsing Kao**, and Tan-Fu Lei, "High performance metal-induced lateral crystallized polycrystalline silicon p-channel thin film transistor with TaN/HfO₂ gate stack structure," *IEEE Electron Device Lett.*, have been accepted for publication.

- [B-6] Ming-Wen Ma, Chin-Yang Chen, Chun-Jung Su, Woei-Cherng Wu, Yi-Hong Wu, **Kuo-Hsing Kao**, Tien-Sheng Chao, and Tan-Fu Lei, "Characteristics of PBTI and hot carrier stress for LTPS-TFT with high- κ gate dielectric," *IEEE Electron Device Lett.*, vol. 29, no. 2, pp.171-173, Feb., 2008.
- [B-7] Ming-Wen Ma, Chin-Yang Chen, Chun-Jung Su, Woei-Cherng Wu, Yi-Hong Wu, Tsung-Yu Yang, **Kuo-Hsing Kao**, Tien-Sheng Chao, and Tan-Fu Lei, "Impacts of fluorine ion implantation with low temperature solid-phase crystallized activation on high- κ LTPS-TFT," *IEEE Electron Device Lett.*, vol. 29, no. 2, pp.168-170, Feb., 2008.

C. International Conference Paper :

- [C-1] Ming-Wen Ma, **Kuo Hsing Kao**, Tien-Sheng Chao and Tan-Fu lei, "Ultra-low temperature of aluminum silicate dielectric formed by nitric acid" 2006 *International Workshop on Dielectric Thin Films for Future ULSI Devices Technical Program*, November, Kawasaki, Japan, pp. 81-82, Nov. 2006.
- [C-2] Ming-Wen Ma, Tsung-Yu Yang, **Kuo-Hsing Kao**, Chun-Jung Su, Tien-Sheng Chao, and Tan-Fu Lei, "Mobility improvement of HfO₂ LTPS-TFTs with nitrogen implantation," *Asia Display 2007 International Conference*, Shanghai, China, pp. 674-677, March, 2007.
- [C-3] Ming-Wen Ma, Tsung-Yu Yang, **Kuo-Hsing Kao**, Tien-Sheng Chao, and Tan-Fu Lei, "Improvement on performance and reliability of TaN/HfO₂ LTPS-TFTs with fluorine implantation," *2007 International Thin Film Transistors Conference*, January, Rome, Italy, pp.352-355, Jan. 2007.
- [C-4] Ming-Wen Ma, Tsung-Yu Yang, **Kuo-Hsing Kao**, Chun-Jung Su, Tien-ShengChao, and Tan-Fu Lei, "High performance LTPS TFTs with HfO₂ gate dielectric and nitric acid pre-treatment," *2006 International Workshop on Dielectric Thin Films for Future ULSI Devices Technical Program*, November, Kawasaki, Japan, pp. 33-34, Nov. 2006.
- [C-5] Ming-Wen Ma, Tien-Sheng Chao, **Kuo-Hsing Kao**, Jyun-Siang Huang and Tan-Fu Lei," Impacts of high- κ .offset spacer on 65-nm node SOI devices",*Ninth International Conference on Modeling and Simulation of Microsystems*, Boston, Massachusetts, pp.697-700, May 2006.
- [C-6] Ming-Wen Ma, Tien-Sheng Chao, **Kuo-Hsing Kao**, Jyun-Siang Huang and Tan-Fu Lei," Novel FD SOI devices structure for low standby power applications", *Ninth International Conference on Modeling and Simulation of Microsystems*, Boston, Massachusetts, pp.59-62, May 2006.
- [C-7] Tsung-Yu Yang, Ming-Wen Ma, **Kuo-Hsing Kao**, Chun-Jung Su, Tien-Sheng Chao, and Tan-Fu Lei, "Impacts of nitric acid oxidation on low-temperature polycrystalline silicon TFTs with high- κ gate dielectric," *Asia Display 2007 International Conference*, Shanghai, China, pp. 519-522, March 2007.

D. Local Conference Paper :

- [D-1] **Kuo-Hsing Kao**, Jian-Hao Chen, Ming-Wen Ma, Tien-Sheng Chao, Reui-Hung Gau, Michael Y. Chiang, Shioh-Huey Chuang, Tan-Fu Lei and Guang-Li Luo “Characterization of CoTiO₃ Thin Films Formed by Sol-Gel Spin Coating with High Temperature Annealing”, SNTDT 2007 Symposium on Nano Device Technology, Hsin Chu, R.O.C.
- [D-2] Ming-Wen Ma, Tien-Sheng Chao, ***Kuo Hsing Kao***, Jyun-Siang Huang, and Tan-Fu lei, “Novel FD SOI devices structure for ultra low leakage applications,” *SNTDT 2006 Symposium on Nano on Nan Device Technology*, Hsin Chu, R.O.C., pp. T05-07, April, 2006.



簡歷 (Vita)

姓名：高國興

性別：男

出生日：1982 年 11 月 10 日

籍貫：山東省 青島市

出身地：台灣 台北市

學歷：國立中興大學物理學系 學士班

2001 年 9 月-2005 年 6 月

國立交通大學電子物理研究所 碩士班

2005 年 9 月-2008 年 6 月



碩士論文題目：

利用溶膠旋轉塗佈法備製鈦酸鈷高介電層

與其材料和物理特性之研究

*A Study on Material and Physical Properties of
CoTiO₃ High-κ Dielectric Prepared by Sol-Gel Spin Coating Method*